An Animal Model for Inherited Human Retinal Dystrophy Caused by the R91W Mutation in Rpe65

DISSERTATION
zur
Erlangung der naturwissenschaftlichen Doktorwürde
(Dr. sc. nat.)

vorgelegt der
Mathematisch-naturwisssenschaftlichen Fakultät
der
Universität Zürich

von

Marijana Samardzija
aus
Kroatien

Promotionskomitee

Prof. Dr. Peter Sonderegger
Prof. Dr. Charlotte Remé
Prof. Dr. Jean-Marc Fritschy

Zürich, 2007

SUMMARY

Background: RPE65, a pigment epithelial protein, is essential for the regeneration of 11-*cis* retinal - the chromophore of both cone and rod visual pigments. Mutations in Rpe65 lead to a spectrum of retinal dystrophies ranging from congenital blindness to autosomal recessive Retinitis Pigmentosa (RP). More than 80 disease-associated mutations have been identified in the Rpe65 gene. According to *in vitro* studies, many of these pathogenic mutations appear to result in a partial or a complete loss of RPE65 function. The most frequent mutation found in patients is an amino acid substitution at position 91 (R91W). Patients carrying this mutation have useful cone-mediated vision in the first decade of life suggesting that the mutant RPE65 protein is still functional. All currently available animal models for RPE65-caused visual defects are functional knock-outs. Therefore, these models cannot reproduce the previously described human pathology caused by missense mutation. I generated an R91W knock-in mouse as a model to understand the mechanism of retinal degeneration caused by aberrant Rpe65 function.

Results: the R91W mutation caused a reduction of RPE65 protein expression. As a consequence, reduced amounts of 11-*cis* retinal and disturbed rhodopsin regeneration kinetics were detected. The insufficient supply of the 11-*cis* retinal to the photoreceptors resulted in retinal degeneration as evidenced by: disturbed photoreceptor morphology, progressive loss of photoreceptor nuclei paralleled by an increase in retinal degeneration markers, and accumulation of abnormal inclusions in the retinal pigment epithelium. Accordingly, electrophysiological measurements showed severely affected photoreceptor responses. After selective ablation of rod activity functional tests revealed that the cone function is preserved at earlier ages in R91W knock-in mice.

The phenotype of R91W knock-in mice was clearly distinctive from that of Rpe65 deficient mouse evidenced by: i) presence of reduced but detectable mutant RPE65 protein ii) presence of 11-*cis* retinal and rhodopsin, and their temporal persistence even in the old animals, iii) better preservation of retinal morphology at least at earlier ages iv) prolonged survival of cones, v) and preserved cone function, which is lost early postnatally in $Rpe65^{-/-}$.

Significance: The R91W knock-in mouse mimics many aspects of the human pathology and thus is a more appropriate model for pre-clinical investigations than the

Rpe65 knock-out mouse. Particularly, the relative longevity of cones in R91W knock-in mice may have dramatic impact on upcoming clinical trials with regard to the therapeutic window in the corresponding patients.

ZUSAMMENFASSUNG

Hintergrund: RPE65 ist ein Protein des retinalen Pigmentepithels, welches das Chromophor für die Stäbchen und Zapfen Sehpigment – Apoproteine generiert. Mutationen im Rpe65 Gen führen zu Netzhautdystrophien mit einer Bandbreite von autosomal rezessiver Retinitis Pigmentosa (RP) bis hin zu Blindheit bei der Geburt. Mehr als 80 Mutationen im Rpe65 Gen führen zur Erkrankung. *In vitro* Studien deuten darauf hin, dass viele dieser Mutationen zu einem teilweisen oder sogar vollständigen Funktionsverlust führen. Die in Patienten am häufigsten gefundene Mutation in Rpe65 führt zu einer Aminosäuresubstitution an Position 91: R91W. Patienten mit dieser Mutation haben brauchbares Zapfensehen während der ersten Lebensdekade, was darauf hindeutet, dass das mutierte RPE65 eine Restfunktion hat. Alle zur Zeit verfügbaren Tiermodelle sind hingegen echte (funktionelle) knock-outs, d.h. sie sind keine geeigneten Modelle für Erkrankungen, die durch eine Missense Mutation wie R91W verursacht werden. Ich habe im Rahmen dieser Arbeit eine R91W knock-in Maus hergestellt, um den Mechanismus der Degeneration bei ungenügender RPE65 Funktion zu untersuchen.

Ergebnisse: Die R91W Mutation führt zu einer Reduktion der RPE65 Protein Expression. Daraus resultiert ein reduzierter 11-*cis* Retinal Gehalt und eine gestörte Kinetik der Rhodopsin Regeneration. Die Unterversorgung mit 11-*cis* Retinal führt zur Degeneration der Netzhaut, was durch folgende Befunde deutlich wird: Gestörte Morphologie der Photorezeptoren, zunehmender Verlust von Photorezeptoren mit einem Anstieg von Degenerationsmarkern und schliesslich eine Zunahme abnormaler Einschlüsse im Pigmentepithel. In Übereinstimmung mit diesen Befunden zeigt sich, dass die Funktion der Photorezeptoren deutlich eingeschränkt ist. Selektive Inhibition der Stäbchenfunktion führte darüberhinaus zu der Erkenntnis, dass die Funktion der Zapfen zumindest in jungen R91W knock-in Tieren erhalten ist.

Dieser Phänotyp unterscheidet sich deutlich von dem der Rpe65 knock-out Maus, wie folgende Parameter belegen: 1) RPE65 Protein ist in der knock-in Maus detektierbar 2) 11-*cis* Retinal und Rhodopsin sind auch in älteren knock-in Tieren messbar 3) Die Netzhautmorphologie ist zumindest in jüngeren knock-in Tieren besser erhalten 4) Zapfen bleiben länger erhalten 5) Zapfenfunktion ist in der knock-in Maus messbar, geht in der knock-out Maus hingegen früh nach der Geburt verloren.

Signifikanz: Die R91W knock-in Maus weist viele Eigenschaften der menschlichen Erkrankung auf, und ist daher als Modell für prä-klinische Studien besser geeignet als die Rpe65 knock-out Maus. Insbesondere die Langlebigkeit der Zapfen in der knock-in Maus könnte einen dramatischen Einfluss auf die anstehenden klinischen Versuche haben, vor allem in Bezug auf das therapeutische Fenster in den entsprechenden Patienten.

CONTENTS

SUMMARY **1**

ZUSAMMENFASSUNG **3**

CONTENTS **5**

1 INTRODUCTION **7**

1.1 PRINCIPLE ORGANIZATION OF THE RETINA 7

1.1.1 Photoreceptors *8*

1.1.2 Retinal pigment epithelium (RPE) *10*

1.2 LIGHT-INDUCED BIOCHEMICAL RESPONSES OF THE RETINA 11

1.2.1 Phototransduction *11*

1.2.2 The visual cycle for retinoid regeneration *13*

1.3 HUMAN RETINAL DYSTROPHIES AND DEGENERATIONS 16

1.3.1 Genes associated with inherited retinal degenerations affecting photoreceptor function *17*

1.3.2 Inherited retinal degenerations caused by mutations in genes of the visual cycle and animal models *18*

1.4 THE RPE65 GENE: RETINOID REGENERATION AND RETINAL DEGENERATION 19

1.4.1 RPE65 involvement in the regeneration of 11-cis retinal *19*

1.4.2 RPE65 mutations in early-onset severe retinal dystrophy (EOSRD) and Leber congenital amaurosis (LCA) *20*

1.5 AIMS OF THE PROJECT 22

2 MATERIALS AND METHODS **23**

2.1 GENERATION OF THE R91W KNOCK-IN MICE 23

2.1.1 RPE65 genomic source DNA *23*

2.1.2 The neomycin (neo) and diphtheria toxin (DT) resistance genes *25*

2.1.3 Site-directed mutagenesis *25*

2.1.4 Design of control and targeting construct *26*

2.1.5 Electroporation of embryonic stem (ES) cells *28*

2.1.6 Assessing the ES cells for homologous recombination *28*

2.1.7 Blastocyst injection, assessment of germ line transmission and crossbreeding *29*

2.2 ANIMALS 30

2.3 RNA ISOLATION, REVERSE TRANSCRIPTION AND QUANTITATIVE REAL-TIME PCR 31

2.4 WESTERN BLOTTING 32

2.5 RHODOPSIN MEASUREMENTS 33

2.6 RHODOPSIN REGENERATION KINETICS 33

2.7 HISTOLOGY 34
2.8 IMMUNOFLUORESCENCE 34
2.9 CONE QUANTIFICATION 35
2.10 HPLC DETERMINATION OF RETINOIDS 35
2.11 ERG FUNCTIONAL TESTS 36

3 RESULTS 37

3.1 GENERATION OF R91W KNOCK-IN MICE 37
3.2 RPE65 EXPRESSION IN THE MUTANT MICE 40
3.3 RETINOID ANALYSIS 42
3.4 RHODOPSIN CONTENT AND REGENERATION 44
3.5 PHOTORECEPTOR FUNCTION IN R91W MUTANT MICE 46
3.6 ASSESSMENT OF RETINAL MORPHOLOGY 49
3.7 CONES ARE FUNCTIONAL IN R91W 52
3.8 REDUCTION IN CONE AND ROD MARKERS 55
3.9 DEGENERATION MARKERS 59

4 DISCUSSION 60

4.1 R91W KNOCK-IN MICE: CLOSE CORRELATION WITH THE HUMAN PHENOTYPE 60
4.2 R91W KNOCK-IN MICE: METABOLIC CHANGES INDUCED BY THE MUTATION 61
4.3 R91W KNOCK-IN MICE: CHANGES IN THE VISUAL CYCLE 62
4.4 CONE LOSS AND DEGENERATION 64

5 REFERENCES 66

ABBREVIATIONS 71

ACKNOWLEDGMENTS 74

CURRICULUM VITAE 75

1 INTRODUCTION

1.1 Principle organization of the retina

The retina is organized in different layers, which contain very specific cell types (Figure 1). Light enters the eye from the anterior segment and first passes the ganglion cell layer (GCL). Ganglion cells are the tertiary neurons of the retina that collect all input from secondary neurons, integrate the signal and transmit it to higher visual centers along the optic nerve. Connections to secondary neurons are made within the inner plexiform layer (IPL). There are three principal neuronal cell types present in the inner nuclear layer (INL): Bipolar cells receive input from photoreceptors and propagate the signal to ganglion cells. The output of bipolar cells onto ganglion cells may be modulated by amacrine cells within the IPL. The input to bipolar cells may be modulated by horizontal cells at the level of the outer plexiform layer (OPL). Bipolar cells and photoreceptors have synaptic contact in the OPL. The outer nuclear layer (ONL) comprises photoreceptor nuclei. Light that has passed all layers described so far, finally reaches the outer segments (OS) of photoreceptors, which contains the light-sensitive visual pigment. Two principal types of photoreceptors – rods and cones – are responsible for dim light vision or color vision, respectively. Behind the photoreceptors follows the retinal pigment epithelium (RPE), which has several functions essential for photoreceptor function and maintenance. RPE and photoreceptors depend on the blood supply provided by the choroid. The other retinal layers are supported by vessels within the retina (not depicted). Müller cells span almost all layers of the retina and have several functions in ionic homeostasis, clearance of neurotransmitters and maintenance of retinal integrity (Figure 1).

The direct route of visual transmission: photoreceptors – bipolar cells – ganglion cells is modulated by lateral interactions of horizontal and amacrine cells. The major focus of this thesis is however placed on two cell types in the retina: the RPE and photoreceptors; which will be discussed in further parts.

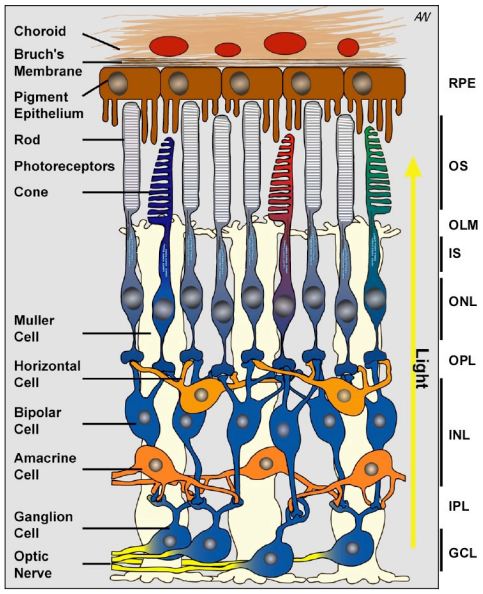

Figure 1 Retinal organization

The retina consists of two principle structures, the neural retina and the retinal pigment epithelium (RPE). The neural retina is arranged in 3 cell layers: i), outer nuclear layer (ONL), containing nuclei of photoreceptors, ii) inner nuclear layer (INL), containing secondary and inter- neurons and iii) the ganglion cell layer (GCL), projecting to the brain. The nuclear layers consist of cell bodies of five basic neuronal cell types: photoreceptors (ONL); bipolar, horizontal and amacrine cells (INL) and ganglion cells (GCL). The processes and synaptic contacts are located in the inner plexiform layer (IPL) and outer plexiform layer (OPL), respectively. Müller cells are the radial glial cells of the retina. The outer limiting membrane (OLM) of retina is formed from adherens junctions between Müller cells and photoreceptor cell inner segments.
IS, inner segments; OS, outer segments of photorecptors.

1.1.1 Photoreceptors

Photoreceptors in the retina are light sensitive cells that convert light into a neuronal signal. The human retina contains two types of photoreceptors, rods and cones. The rods outnumber the cones, 110–125 million vs. 6 million, respectively (Osterberg 1935). The distribution of rods and cones throughout the human retina varies from periphery to the center, in contrast to non-primate species. The macula, the central portion of the retina, is characterized by a high density of photoreceptors. In its center is the fovea, an area containing exclusively cone photoreceptors. Approximately 200’000 cones are found in the fovea. This cone-rich area is responsible for clear and sharp central color vision.

The basic anatomy of rods and cones is shown schematically in Figure 2. Both photoreceptor types consist of a cell body with the synaptic terminus on one side and the inner segment containing the metabolic machinery of the cell (the mitochondria, Golgi apparatus, endoplasmic reticulum etc.) on the opposite side. The outer segment of rods, which extends from the inner segment, contains a stack of about 1000 membrane discs, containing the photopigment rhodopsin (Figure 2) (Forrester et al. 1996). Cones have no disks; instead surface enlargement is achieved by infoldings of the plasma membrane. Cones possess less photopigments per cell than rods.

Each photoreceptor cell has a single type of photopigment composed of a protein opsin (rod-, cone- and color-specific) to which the chromophore 11-*cis* retinal is

covalently bound. Rods express only one type of opsin and their photopigment rhodopsin has a maximal spectral sensitivity at 496 nm (Dartnall et al. 1983). Three kinds of cone pigments are expressed in human retinas: red- (long, 558 nm), green- (middle, 531 nm) and blue-sensitive pigment (short, 419 nm) representing maximal sensitivity to red, green or blue light, respectively (Dartnall et al. 1983). Rod photoreceptors are highly sensitive to light of low intensity and therefore the rod system is optimized for sensitivity at the expense of resolution. Cones, however, function predominantly in bright light where they are involved in detecting color. The cone system, especially in the fovea, provides high spatial resolution and is specialized for acuity at the expense of sensitivity. In extreme illumination conditions (dim light as opposed to bright light) basically two types of photoreceptor responses exist: i) under conditions of low luminance exclusively rods are sufficiently sensitive to respond. This rod-mediated perception is called scotopic vision. ii) Conversely under bright light conditions, responses of rods are saturated, and only cones contribute to vision. This type of vision is termed photopic vision. In intermediate lighting conditions a mixed response occurs. This type of vision is called mesopic vision. Functionally, these properties of photoreceptors can be tested by electroretinography (ERG), which measures the light-evoked electrical responses of various cell types in the retina in addition to the photoreceptors.

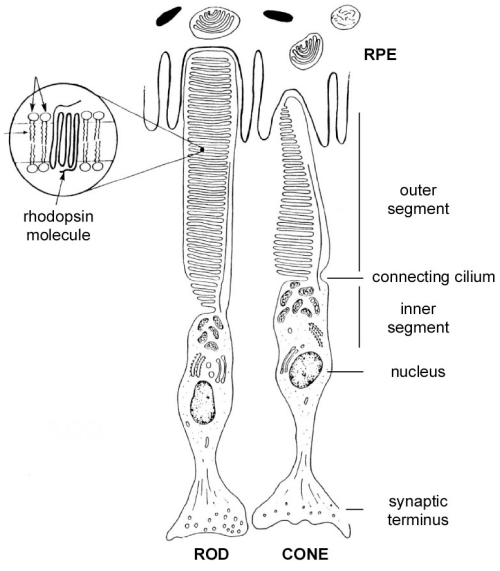

Figure 2 Photoreceptor structural organization

Rods and cones share many structural features and both are extremely polarized cells. Both have synaptic terminals connected to the soma located within the ONL. The lumen of the soma is almost entirely occupied by the nucleus. Endoplasmic reticulum and mitochondria are displaced into the inner segment. Any protein synthesized here has to be transported through the connecting cilium to reach the outer segment. In the case of rods, the outer segments contain densely packed discs, which increase the area for high-density packing of the visual pigment in an orientation allowing maximal photon catch. In cones, OS membranes are not organized as separate disks but are continuous, invaginating from the plasma membrane. The tip of each photoreceptor is surrounded by RPE-villous processes to enable the efficient exchange of nutrients, vitamin A and photoreceptor renewal.

1.1.2 Retinal pigment epithelium (RPE)

The RPE, located immediately behind the photoreceptors, is a single layer of cells, which was termed pigmented due to its large content of melanin pigment. This pigmentation influences vision physically by eliminating light scattering.

The RPE is involved in many aspects of outer retinal metabolism that are essential for the continued maintenance of the photoreceptor cells such as: protection against photo-oxidation, transport of nutrients between photoreceptors and the choriocapillaris, buffering of ions in the subretinal space, secretion of trophic factors etc. The apical side of the RPE cells with their microvilli surrounds the tips of photoreceptor cells (Figure 1 and 2), creating a large surface for exchange between the two cell types. Probably the two most important features of the RPE are phagocytosis of shed photoreceptor tips and regeneration of the visual pigment chromophore. Photoreceptor exposure to intense light levels leads to accumulation of high concentration of radicals, photo-damaged proteins and lipids in the tips of their outer segments. These tips are shed diurnally and phagocytosed by the RPE. In turn, the outer segments are renewed on their basal side, at the connecting cilium (Figure 2). It is estimated that the turnover rate - the time needed to form an entirely new photoreceptor outer segment - in the primate retina takes about 10 days (Young 1971). The shed tips are digested in the RPE and critical molecules are recycled and returned back to the photoreceptors. With age this complex process appears to slow down, possibly contributing to blinding diseases such as age-related macular degeneration (AMD).

Regeneration of the visual pigment chromophore, another kind of recycling in the RPE, will be discussed in the following section.

1.2 Light-induced biochemical responses of the retina

The visual pigment in rod cells, rhodopsin, consists of the transmembrane protein opsin covalently bound to the chromophore 11-*cis* retinal. Opsin has seven membrane-spanning helices, similar to other receptors that interact with transducing G proteins. Rhodopsin is localized to the flattened membrane disks that are piled in the rod's outer segment (Figure 2).

In the resting state, cyclic-nucleotide-gated channels (CNG) in rod plasma membrane are open, allowing the simultaneous inward flux of Na^+, Ca^{2+}, and K^+ ions (Figure 3). As a result the membrane potential of a resting rod cell is about -37 mV (Schneeweis and Schnapf 1995), which is considerably lower than the resting potential typical of neurons (-60 to -90 mV). Due to this constant depolarization, dark-adapted rod cells are constantly secreting the neurotransmitter glutamate. Depending on the type of the downstream bipolar cell, the glutamate stimulates the OFF-pathway or inhibits the ON-pathway, respectively. With no excitatory neurotransmitter release from bipolar cells, ganglion cells are also turned off.

When a photon of light reaches the photoreceptor outer segment a series of molecular events culminating in an electrical response is induced. The primary photochemical event is isomerization of the 11-*cis* retinal in rhodopsin to all-*trans* retinal. In the following text two separate processes induced by light are described.

1.2.1 Phototransduction

Phototransduction is the process by which the energy of a photon of light is converted in the photoreceptor cell outer segment into a neuronal signal e.g. a change of a transmembrane potential (reviewed in (Burns and Baylor 2001; Arshavsky et al. 2002)). Light absorption leads to the photoisomerization of 11-*cis* retinal to all-*trans* retinal causing a physical change in the opsin moiety of rhodopsin leading to a conformational state called metarhodopsin II. Metarhodopsin II activates the photoreceptor-specific G protein, transducin. Transducin is a heterotrimeric protein that in its inactive state is composed of α, β and γ subunits (Figure 3). Metarhodopsin II activation results in the fast exchange of GDP for GTP on the α subunit of transducin causing release of the β and the γ subunit. The GTP bound α subunit of transducin

causes activation of a phosphodiesterase (PDE) (Figure 3). The PDE is a heterotetramer composed of two catalytical subunits and two identical regulatory subunits (PDEγ). The role of the PDEγ subunit is to maintain the PDE in a nonactivated state. The activated α subunit of transducin binds to the PDEγ subunit resulting in the activation of the two catalytic subunits of PDE. Its activation results in the degradation cGMP to GMP (Figure 3). The decrease in cGMP concentration leads to the closure of the CNG channels. The closure of the CNG channels results in a decrease in cation influx and as the export of Ca^{2+} continues for additional 1 sec, this causes a hyperpolarization of the cell (Figure 3). This complex biochemical cascade initiated by photon capture provides enormous signal amplification. It has been estimated that the absorption of a single photon by a rhodopsin molecule causes a net change in the membrane potential of about 1 mV (Schneeweis and Schnapf 1995). The amplification-factor is about 1 million and makes photoreceptors the ultimate sensory neurons as they are able to detect and respond to a single photon (Baylor et al. 1979)

Accompanying the light induced hyperpolarization, decreased influx together with continuous export of Ca^{2+} lowers the intracellular Ca^{2+} concentration, leading to adaptational changes in the phototransduction cascade, all of which tend to reduce the sensitivity of the receptor to light. The combination of these adaptive mechanisms allows the retina to function at light intensities differing by 10 log units (reviewed in (Reme et al. 1991)).

In order to quickly restore the system's basal state all the activated intermediates (metarhodopsin II, α subunit of transducin and activated PDE) need to be inactivated rapidly. Lowered intracellular Ca^{2+} concentration disinhibits guanylate-cyclase-activating protein (GCAP), leading to the activation of guanylate cyclase (GC) and thus resynthesis of cGMP. PDE is inactivated by the hydrolysis of the GTP bound to the α subunit of transducin allowing re-formation of the transducin trimer and release of PDE. Rhodopsin is phosphorylated by rhodopsin kinase (RK) and inactivated by binding of arrestin. The protein arrestin blocks the ability of activated rhodopsin to interact with transducin, and also facilitates the release of all-*trans* retinal (the opsin agonist) from the opsin. The released all-*trans* retinal then enters an elaborate recycling system: the visual cycle.

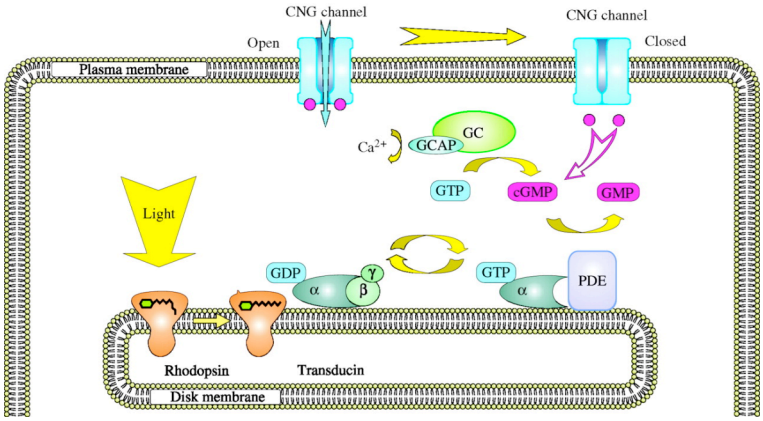

Figure 3 A schematic representation of the phototransduction cascade in the rod outer segments of vertebrates.

Phototransduction in rod photoreceptors starts with the absorption of a photon by the visual pigment rhodopsin, which sits in the membrane of the disc. The absorption triggers a conformational change first in the chromophore (11-*cis* to all-*trans*) and subsequently in the protein moiety, the opsin. This change allows the binding of transducin, which now exchanges GDP for GTP and sheds its two inhibitory subunits gamma and beta. Activated transducin triggers activation of PDE, which starts hydrolyzing cGMP and thus quickly removes the ligand of the CNG channel at the cell surface. Upon channel closure, the membrane potential of the photoreceptor hyperpolarizes – a light signal has been converted into an electrical signal that is interpretable by neurons. Following cessation of the stimulus, cGMP levels are restored by the activity of GC, which below a certain level of free Ca^{2+} becomes activated by GCAPs. The transduction cascade is amplified by about 1 million times and can be modulated at several levels.
cGMP, cyclic GMP; CNG, cyclic nucleotide gated; GC, guanylate cyclase; GCAP, guanylate-cyclase-activating protein; GDP, guanosine diphosphate; GMP, guanosine monophosphate; GTP, guanosine triphosphate, PDE, phosphodiesterase.
Taken from (Kramer and Molokanova 2001)

1.2.2 The visual cycle for retinoid regeneration

Photoisomerisation (bleaching of rhodopsin) of 11-*cis* retinal to all-*trans* retinal causes the dissociation of all-*trans* retinal from the opsin molecule. The restoration of light sensitivity of the bleached opsin requires regeneration of 11-*cis* retinal through an enzymatic pathway called the visual cycle. Several enzymatic steps are required to convert all-*trans* retinal to 11-*cis* retinal and the biochemical reactions that carry out the *trans* to *cis* conversion are confined to the RPE (Redmond et al. 1998) (Figure 4). After photon absorption and release from the opsin molecule, all-*trans* retinal is transported out of rod disc membrane by a retina-specific ATP-binding cassette protein (ABCR) to the cytoplasm. All-*trans* retinol dehydrogenase (atRDH) reduces the aldehyde to all-*trans* retinol. All-*trans* retinol is then released from the outer segments of the

photoreceptor cells, bound to the inter-photoreceptor retinol binding protein (IRBP) and carried into the RPE. Once inside the RPE, all-*trans* retinol is bound to cellular retinol binding protein (CRBP) (Saari et al. 1982) (Figure 4). A transferase enzyme, lecithin retinol acyl transferase (LRAT), esterifies the all-*trans* retinol to produce all-*trans* retinyl ester (Saari and Bredberg 1989; Trehan et al. 1990). This ester form is the substrate for RPE65 that acts as an isomerohydrolase (IMH) catalyzing the hydrolysis of all-*trans* retinol and subsequent isomerization into 11-*cis* retinol (Jin et al. 2005; Moiseyev et al. 2005; Redmond et al. 2005). 11-*cis* retinol dehydrogenase (11cRDH) then oxidizes 11-*cis* retinol to 11-*cis* retinal (Simon et al. 1995) in a reaction accelerated by the presence of cellular retinaldehyde binding protein (CRALBP) (Saari et al. 2001).

Finally, 11-*cis* retinal is transported back to the photoreceptor and the opsin molecule. During the regeneration process, the derivatives of retinol (retinoids) are bound by retinoid-binding proteins (IRBP, CRBP, CRALBP) to solubilize the hydrophobic retinoids and to protect them from oxidation.

After it is transported back into the outer segment, the 11-*cis* retinal recombines with opsin in the receptor disks (Figure 4).

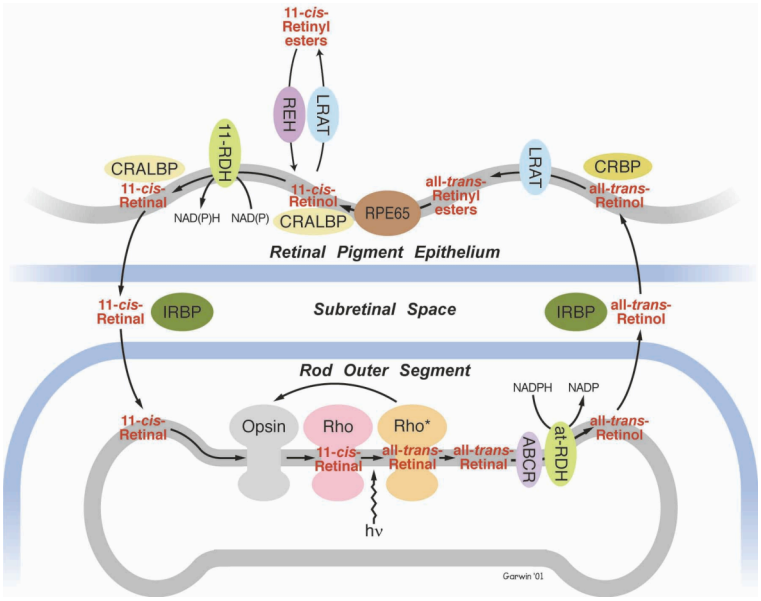

Figure 4 The visual cycle

Upon photon absorption 11-*cis* retinal is converted into all-*trans* retinal and released into the disc lumen. The transport across the disc membrane is facilitated by ABCR and the aldehyde is reduced into all-*trans* retinol by an atRDH. All-*trans* retinol leaves the photoreceptor by so far unknown mechanisms and is chaperoned by IRBP in the extracellular space. It enters the RPE – again by unknown mechanisms – in the lumen of which it is chaperoned and transported by CRBP. All-*trans* retinol is esterified to a fatty acid by LRAT. The resulting all-*trans* retinyl ester is the storage form for vitamin A in the eye and the substrate for RPE65 hydrolysing the all-*trans* retinol from the ester and inducing the re-isomerization to 11-*cis* retinol. 11-*cis* retinol binds to CRALBP and in a subsequent step is oxidized by a 11cRDH to form 11-*cis* retinal. Alternatively, 11-*cis* retinol may be esterified by LRAT to yield 11-*cis* retinyl esters, a storage form of pre-isomerized retinoid. 11-*cis* retinyl esters are hydrolyzed to 11-*cis* retinal by 11cREH, which is not yet cloned. 11-*cis* retinal leaves the RPE, is chaperoned by IRBP during its transport back to the photoreceptor and - by unknown mechanisms – reaches the naked opsin to restore its light-sensitivity.
11cRDH, 11-cis retinol dehydrogenase; 11cREH, 11-cis retinyl ester hydrolase; ABCR, ATP-binding cassette retina; atRDH; all-trans retinol dehydrogenase; CRALBP, cellular retinaldehyde binding protein; CRBP, cellular retinol binding protein; IRBP, inter-photoreceptor retinol binding protein; LRAT, lecithin retinol acyl transferase; RPE, retinal pigment epithelium

1.3 Human retinal dystrophies and degenerations

Retinal dystrophies and degenerations can be caused by genetic or non-genetic factors, and typically affect specific cell types within the retina.

Age-related macular degeneration (AMD) is a degenerative retinal disease specifically affecting the macula of elderly people. The macula is the central, cone-rich region of the retina that is responsible for clear and sharp central vision. As a general rule, AMD is causing severe visual impairment characterized by poor visual acuity and impaired color vision. AMD is a major leading cause of blindness in the aged population over 60. AMD is a multifactorial disorder that is associated with environmental risk factors such as cigarette smoking, nutrition, life-long exposure to light, and cholesterol level. However, it has been recently established that genetic factors also contribute to pathogenesis of AMD. Independent studies suggested that missense mutations in complement factor H (CFH) may lead to AMD with a prevalence close to one half of all AMD disease cases (Conley et al. 2005; Edwards et al. 2005; Hageman et al. 2005; Haines et al. 2005; Klein et al. 2005; Zareparsi et al. 2005). Another study showed that variation in factor B (BF) and complement component 2 (C2) genes may be additional risk loci for AMD (Gold et al. 2006). Collectively, these data point to a causative role of the immune system in the development of AMD. In addition, the PLEKHA1/LOC387715 locus within 10q26 has been described as a possible second major locus contributing to AMD development (Jakobsdottir et al. 2005; Rivera et al. 2005).

Retinal dystrophies are a genetically and phenotypically diverse group of inherited diseases that lead to visual impairment, affecting all age groups and ethnic backgrounds. Based upon clinical symptoms, ERG, and/or genetical similarities a common grouping has been made to classify retinal diseases. I.e. retinitis pigmentosa (RP) is a collection of progressive inherited disorders in which abnormalities of the photoreceptors (rods and cones) or the RPE lead to progressive visual loss. The mode of inheritance in RP may be autosomal dominant, autosomal recessive, X-linked, or mitochondrial. RP is characterized by initial loss of rods, resulting in night blindness, constricted visual fields, and fundus alterations. While AMD, primarily affecting the macula, rarely results in complete blindness, hereditary retinal degenerations that affect the whole retina tend to be more severe. More than 170 gene loci have been associated with retinal dystrophies (http://www.sph.uth.tmc.edu/Retnet/disease.htm).

Most of these genes are specifically expressed in the retina, particularly in photoreceptors.

1.3.1 Genes associated with inherited retinal degenerations affecting photoreceptor function

Retinal dystrophies, which include RP, form one of the largest single cause of inherited blindness in the developed world. RP affects about 1 in 3500 people worldwide. Mutations in rhodopsin gene are the most common cause of RP. The P23H mutation in rhodopsin was the first gene mutation shown to cause RP, accounting for 12% of the adRP population in the US (Dryja et al. 1990; Sung et al. 1991). Mutations in the rhodopsin gene can lead to adRP, arRP or congenital stationary night blindness (CSNB) (illustrated in Figure 5). This phenotypic divergence is called allelic heterogeneity. On the other hand mutations in different genes can lead to similar phenotype; i.e. CSNB can result from mutations in rhodopsin, transducin, arrestin etc. Most genes associated with RP encode proteins involved in phototransduction, the visual cycle, photoreceptor structure and transcription factors.

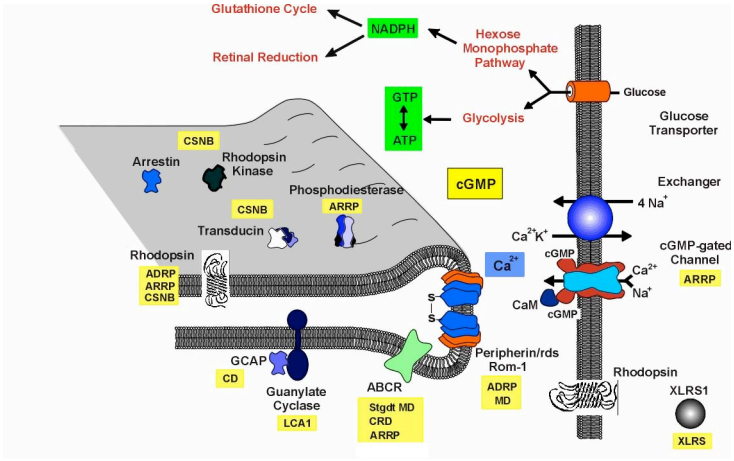

Figure 5 A brief overview of photoreceptor-related proteins linked to various types of retinal diseases

Several examples of genes involved in the phototransduction cascade, photoreceptor structure, metabolism or morphogenesis and their connection to disease.

ADRP, autosomal dominant RP; ARRP, autosomal recessive RP; CD, cone dystrophy; CRD, cone-rod dystrophy; CSNB, congenital stationary night blindness; LCA1, Leber congenital amaurosis type 1; MD, macular degeneration; RP, retinitis pigmentosa; Stgdt, Stargardt; XLRS, X-linked retinoschisis.

Adapted from http://www.biochem.ubc.ca/fac_research/faculty/molday.html

1.3.2 Inherited retinal degenerations caused by mutations in genes of the visual cycle and animal models

Sustained visual function depends on a functional visual cycle replenishing the vitamin A derivative - 11-*cis* retinal - to the opsin molecule. Defects in Vitamin A metabolism in the RPE may result in dysfunction and degeneration of the retina.

Table 1 Visual cycle genes in conjunction with human eye diseases and animal models

Enzyme/ protein	*Abbrev.*	*Gene*	*Human disease(OMIM; RetNet)*	*Mouse model*
All-trans retinol dehydrogenase	atRDH	*RDH8 (prRDH)*	no	KO (Maeda et al. 2005)
ATP-binding cassette retina	ABCR	*ABCA4*	Stargardt disease, arMD; arRP; ar fundus flavimaculatus; ar cone-rod dystrophy;	KO (Weng et al. 1999)
Inter-photoreceptor retinol binding protein	IRBP	*RBP3*	no	KO (Liou et al. 1998)
Cellular retinol binding protein	CRBP	*RBP1*	no	KO (Ghyselinck et al. 1999)
Lecithin retinol acyl transferase	LRAT	*LRAT*	LCA, EOSRD	KO (Batten et al. 2004) (Liu and Gudas 2005)
RPE65	RPE65	*RPE65*	LCA, arRP, EOSRD	KO (Redmond et al. 1998), rd12 (Pang et al. 2005), Briard dog (Aguirre et al. 1998)
11-cis retinol dehydrogenase	11cRDH	*RDH5*	ar fundus albipunctatus; ar cone dystrophy,	KO (Driessen et al. 2000)
Cellular retinaldehyde binding protein	CRALBP	*RLBP1*	ar RP, ar retinitis punctata albescence, ar Bothnia dystrophy, ar cone-rod dystrophy	KO (Saari et al. 2001)
Retinal G-protein-coupled receptor	RGR	*RGR*	arRP, adRP	KO (Chen et al. 2001)

ad, autosomal dominant; ar, autosomal recessive; EOSRD, early-onset severe retinal dystrophy; LCA, Leber congenital amaurosis; MD, macular degeneration; RP, retinitis pigmentosa; KO, Knock-out (http://www.ncbi.nlm.nih.gov/entrez/query.fcgi?db=OMIM; http://www.sph.uth.tmc.edu/Retnet/disease.htm)

Genetic models developed to study visual cycle genes revealed that defects in RPE-specific genes might result in photoreceptor cell loss as a primary event, and vice versa. I.e. defects in genes expressed in the RPE – such as Rpe65 and MerTK (c-mer proto-oncogene tyrosine kinase) – primarily result in photoreceptor degeneration. On the other hand, a defect in a gene exclusively expressed in photoreceptors – ABCR - leads to RPE degeneration. Such close interdependence between photoreceptors and RPE led to the consideration of RPE and photoreceptors as a one functional unit. The metabolic processes in the RPE are very complex, and many of the proteins involved in the visual cycle are not identified or fully characterized. Table 1 shows proteins of established function in the visual cycle in connection to human disease and developed animal models. Patients with mutations in atRDH (RDH8), IRBP (RBP3) and CRBP (RBP1) have not been reported so far.

1.4 The Rpe65 gene: retinoid regeneration and retinal degeneration

Nicoletti et al. characterized the human Rpe65 gene and mapped it to chromosome 1 (Nicoletti et al. 1995). The Rpe65 gene consists of 14 exons spread over 20 kilobase pairs encoding the abundant 61-kDa protein of the retinal pigment epithelium (Hamel et al. 1993b). This protein constitutes up to 50% of the total microsomal protein amount in the RPE cells (Hamel et al. 1993a). Protein sequence comparison revealed high evolutionary conservation of RPE65 with mouse and human protein being 94% identitical.

Together with recently crystallized apocarotenoid-15,15-oxygenase (ACO) from Synechocystis sp., RPE65 belongs to a family of retinal-forming carotenoid oxygenases (Kloer et al. 2005). As in ACO, four conserved histidines coordinating an iron atom are required for its catalytic activity (Poliakov et al. 2005; Redmond et al. 2005).

1.4.1 RPE65 involvement in the regeneration of 11-cis retinal

Studies on RPE65 deficient mice revealed that RPE65 is necessary for the production of the visual chromophore 11-*cis* retinal in the visual cycle. Namely, RPE65 deficient animals show over-accumulation of retinyl esters in RPE and undetectable levels of rhodopsin / 11-*cis* retinal, indicating a blockade of the visual cycle.

Recently, Jin at all (Jin et al. 2005) employing an unbiased cDNA expression screen identified RPE65 as isomerase and by demonstrating catalytic activity in mammalian and insect cells confirmed its enzymatic function in the visual cycle. Additional studies have confirmed the role RPE65 as the isomerohydrolase in the retinoid visual cycle (Moiseyev et al. 2005; Redmond et al. 2005). Furthermore, mutational analysis of iron-binding histidine residues, based on analogy with other carotenoid oxygenases, identified that the iron-coordinating residues of the RPE65 are essential for its catalytic activity and stability (Redmond et al. 2005; Takahashi et al. 2005).

1.4.2 RPE65 mutations in early-onset severe retinal dystrophy (EOSRD) and Leber congenital amaurosis (LCA)

More than 80 disease-associated mutations have been identified in the Rpe65 gene so far (for a full list see (Zernant et al. 2005)). The broad spectrum of mutations includes point mutations, splice-site defects, rearrangements, deletions, and insertions. Mutations in Rpe65 are inherited in a recessive manner and it is estimated that they account for approximately 11% of all autosomal recessive childhood-onset retinal dystrophy cases (Thompson et al. 2000). The patients suffering from mutations in the Rpe65 gene are diagnosed as arRP (autosomal recessive), juvenile RP, EOSRD (early-onset severe retinal dystrophy) or LCA (Leber congenital amaurosis). This rather unclear nomenclature reflects the phenotypic heterogeneity underlying the disease (as in many RP cases), but to a certain extent it results from nonuniform diagnostic criteria used by clinicians. RP is the diagnosis given to patients with photoreceptor degeneration who have good central vision within the first decade of life, and the diagnosis of LCA is given to patients who are born blind or lose vision within a few months after birth. Most patients suffering from mutations in the Rpe65 gene are diagnosed early in childhood as severely visually impaired, with congenital night blindness and nystagmus, and no photophobia. Early in infancy patients have severely restricted visual fields, with nondetectable dark-adapted ERG and severely diminished light-adapted ERGs. Most of the patients have useful vision in the first decade of life sufficient to attend elementary school. However, vision is gradually lost resulting in blindness almost invariably in the third decade of life.

Two naturally occurring (rd12 mouse and Briard dog) and the genetically engineered RPE65 knock-out mouse ($Rpe65^{-/-}$) models reported so far have been useful in the delineation of the RPE65 protein function in the visual cycle. These models have meanwhile been used in gene replacement therapy experiments to restore rod and cone photoreceptor function. The above models represent a “null situation” in which the visual cycle has never been functional due to the lack of 11-*cis* retinal synthesis - as a result of the absence of functional RPE65 protein. However, more than 60% of Rpe65 mutations reported in patients are missense mutations. Some of the missense mutations presumably produce mutant versions of the encoded protein with some residual function. This hypothesis is supported by the *in vitro* analysis of mutations associated with LCA / EOSRD. These mutations cause partial or total loss of isomerization activity, which is in direct relation to their clinical effect (Redmond et al. 2005). It is not clear how missense mutations contribute to the human pathology.

Recently, three consanguineous families carrying the R91W mutation in Rpe65 have been characterized (see Figure 6) (El Matri et al. 2006). All affected family members were homozygous for the mutation. The pathology reported is in line with the typical clinical picture described above for EOSRD but not LCA. As the R91W mutation is described as the most common missense mutation in the Rpe65 gene (Thompson et al. 2000) and as the pathology caused by it may not be accessible in the knock-out animal models described so far, it was of importance to develop a model mimicking the disease caused by this missense mutation.

Figure 6 Fundus color photography from patients affected by R91W mutation in Rpe65 gene

Two patterns identified in R91W patients representing earlier (pattern 1) and later (pattern 2) stages of disease. Pattern 1: Confluent white dot deposits, grey discoloration of the RPE and peripapillary atrophy. Pattern 2: Mid-peripheral pigmented clumps of different sizes either entirely pigmented or with central depigmentation.
Adapted from (El Matri et al. 2006)

1.5 AIMS OF THE PROJECT

The R91W mutation is the most common missense mutation in Rpe65 reported in human patients (Thompson et al. 2000). Patients affected by this mutation have useful vision in the first decade of life discriminating them from LCA patients (null mutation in Rpe65) that are blind from birth. All available RPE65 animal models are functional knock-out models and thus models for LCA. It is not known how missense mutations contribute to the pathology. Mouse and human Rpe65 share 94% identity and position 91 is in one of the most conserved regions in the RPE65 protein.

The present work was elaborated in order to mimic human retinal dystrophy caused by a missense mutation in RPE65 thereby providing a tool to study molecular mechanisms of the human disease process that may ultimately lead to blindness. To do so, following steps were undertaken:

- generation of RPE65-R91W knock-in mouse
- characterization of the visual cycle in mutant mice
- visual function assessment
- analysis of the resulting pathology
- comparison to the null situation

2 MATERIALS AND METHODS

2.1 Generation of the R91W knock-in mice

In order to generate a mouse carrying the R91W mutation in the Rpe65 gene, a strategy using homologous recombination (HR) in embryonic stem (ES) cells has been employed to replace the wild-type with a modified Rpe65 gene. The replacement (targeting) vector was designed to possess several basic features: i) a substantially large stretch of genomic DNA containing the desired mutation leading to the R91W substitution to be introduced by HR; ii) a positive selection marker (neomycin resistance gene, neo), which was flanked by loxP sites in order to enable cre-mediated deletion of neo in further steps; iii) a negative selection marker (diphtheria toxin, DT) cassette; iv) a single restriction site in the plasmid backbone of the targeting vector for linearization (XhoI), and v) a marker for detection of the HR event (PCR and Southern blotting). A PCR-based approach was used as a primary screening method. Two constructs have been prepared: a targeting and a control construct. The general strategy applied is shown in Figure 9. Mice were generated in collaboration with Dr. Birgit Lederman (University of Zurich, Zurich, Switzerland).

2.1.1 RPE65 genomic source DNA

Genomic DNA used in our experiment was derived from the 129/Sv mouse strain and consisted of 2.7 kb of the 5' flanking region followed by the first 6 exons with intervening introns of the Rpe65 gene. These 12.7 kbs were divided in two contiguous subclones: E1-12 containing exons 1-3 and clone E2-8 containing exons 4-6 (Figure 7A); cloned into EcoRI restriction site of pBluescriptII SK(-) vector (provided by T.M. Redmond, National Eye Institute, Bethesda, USA) (Boulanger et al. 2001).

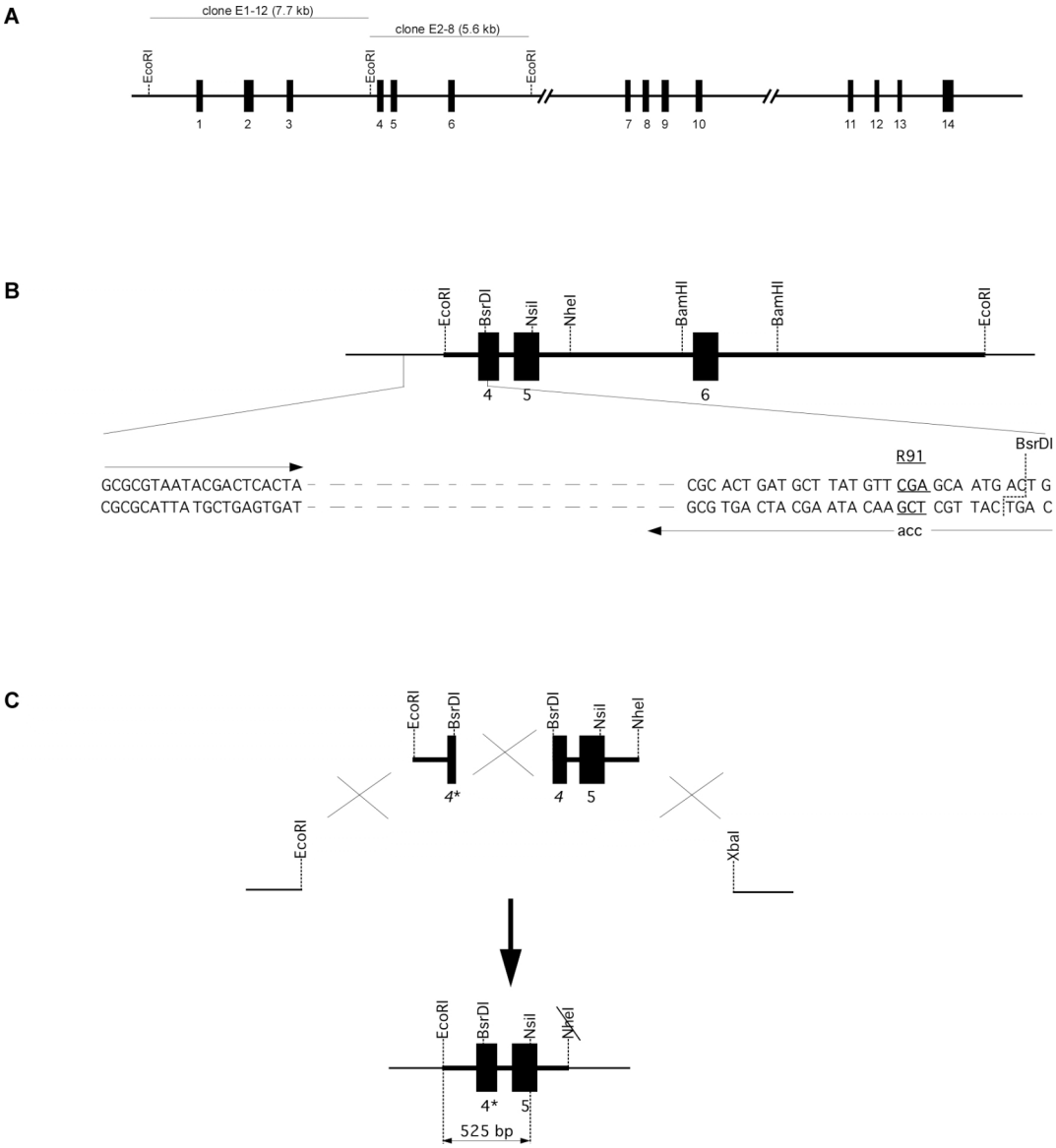

Figure 7 Rpe65^{R91W} site-directed mutagenesis

A, Genomic organization of the mouse Rpe65 gene. Two contiguous clones: E1-12 and E2-8 cloned into EcoRI restriction site of pBluescript II SK(-) containing the first six exons served as source of genomic DNA used for construction of the targeting vector. B, Clone E2-8 containing exons 4-6, was used as template for site-directed mutagenesis. The forward primer was designed to hybridize in the plasmid backbone. The degenerate reverse primer contained two point mutations spanning codon 91 of Rpe65 (indicated in lowercase letters) and spanned a BsrDI restriction site suitable for excision of mutated fragment. The PCR fragment was cloned into PCR2.1-TOPO vector. C, Triple ligation to introduce the R91W mutation into exon 4: The EcoRI/BsrDI (281 bp) restriction fragment derived from site-directed mutagenesis was ligated with the BsrDI/NheI (626 bp) restriction fragment containing the partial exon 4 and exon 5 of the genomic Rpe65 DNA and subcloned into the EcoRI/XbaI polylinker region of the pCR2.1-TOPO vector. Ligation of the complementary XbaI and NheI sticky ends resulted in loss of the NheI site in genomic sequence. For the introduction of the R91W mutation into the targeting vector the EcoRI/NsiI (525 bp) restriction fragment has been excised.

* denotes presence of R91W mutation in exon 4.

2.1.2 The neomycin (neo) and diphtheria toxin (DT) resistance genes

The Neo cassette flanked by mutant loxP sites (floxed-neo) in the direct repeat orientation and the diphtheria toxin (DT) negative selection marker were obtained from A. Zurlinden (University of Zurich, Zurich, Switzerland). Prior to integration of this cassette into the Rpe65 DNA, a Klenow fill-in reaction followed by blunt-end ligation was used to remove the BamHI and EcoRI restriction sites from the floxed-neo cassette. Since further cloning steps required the use of the respective enzymes, this step greatly facilitated the cloning procedure.

2.1.3 Site-directed mutagenesis

Clone E2-8 served as template for the PCR targeted site-directed mutagenesis (Figure 7B). In humans, transition of arginine to tryptophan at position 91 (R91W) is caused by a single point mutation (TGA>TGG) in the Rpe65 gene. Mouse and human codons differ for the respective arginine. Two point mutations were introduced into the mouse R91 codon (CGA>TGG) using a respective reverse primer (C AGT CAT TGC CCA AAC ATA AGC ATC AGT GCG GAT GAA TCT GAA GAC TAT TGA GAA ATG GA; underlined codon denotes position 91) to obtain the R91W mutation (Figure 7B). The forward primer was designed in the plasmid backbone (GCG CGT AAT ACG ACT CAC TA). The PCR was performed with proofreading DyNAzyme EXT DNA Polymerase (Fynnzyme, Espoo, Fi) and PCR conditions were as follows: the initial denaturation at 94 ^{o}C for 4 min, followed by 30 cycles (94 ^{o}C/30 sec; 62 ^{o}C/45 sec and 72 ^{o}C/45 sec) and final extension at 72 ^{o}C for 10 min. The specificity of the PCR reaction was verified by gel electrophoresis, which revealed the expected 363 bps band and no additional products.

The PCR product containing R91W was ligated into a PCR2.1-TOPO vector (#45-0641, Invitrogene, Basel, Switzerland) according to the manufacturer's protocol and propagated in TOP10 One Shot (Invitrogene, Basel, Switzerland) chemically competent bacterial cells. Plasmid DNA was isolated from bacterial cultures using the QIAprep Spin Miniprep Kit (#27106, Qiagen, Basel, Switzerland). The insert was verified by restriction enzyme digestion and sequencing resulting in one positive clone containing the correct sequence. The EcoRI/BsrDI (281 bp) fragment excised from the positive clone and a BsrDI/NheI (626 bp) fragment containing the partial exon 4 and exon 5 of the genomic Rpe65 DNA were subcloned into the EcoRI/XbaI polylinker

region of the pCR2.1-TOPO vector (Figure 7C). This triple ligation step used complementarity of XbaI and NheI sites that resulted in loss of the NheI site in the genomic sequence. Finally, the EcoRI/NsiI (525 bp) fragment containing the R91W mutation was prepared for reintroduction into the targeting construct (see Figure 8; STEP 2B).

2.1.4 Design of control and targeting construct

A single NheI restriction site in clone E2-8 approximately 650 bps downstream of the codone 91 in exon 4 was used for the integration of the neo cassette. The neo cassette was excised by XbaI and ligated into complementary NheI site of E2-8 plasmid producing a control construct (Figure 8; STEP 1). This control construct was used to establish the PCR conditions for HR screening (see section 2.1.6) and for further construction of the targeting vector.

In the following step Rpe65 DNA containing the integrated neo cassette was truncated at the 3' region (Figure 8; STEP 2a) and an EcoRI/NsiI DNA fragment containing the R91W mutation was introduced (Figure 8; STEP 2b). This resulted in the so-called short arm of the targeting vector. For the long arm of the targeting construct the 5' region containing exons 1-3 (from vector E1-12) were ligated to the EcoRI site of the short arm (Figure 8; STEP 3). In the final step the DT cassette was introduced (Figure 8; STEP 4) to serve as a negative selection marker. A single XhoI site in the plasmid backbone was used for linearization prior to electroporation. Each step of ligation was verified by digestion with different restriction enzymes. A restriction pattern was predicted from sequences published in the MGI database (http://www.informatics.jax.org/) and NCBI nucleotide database (http://www.ncbi.nlm.nih.gov/entrez/query.fcgi?db=Nucleotide). To make sure that the targeting vector was correctly constructed, the final targeting construct carrying the R91W mutation was sequenced.

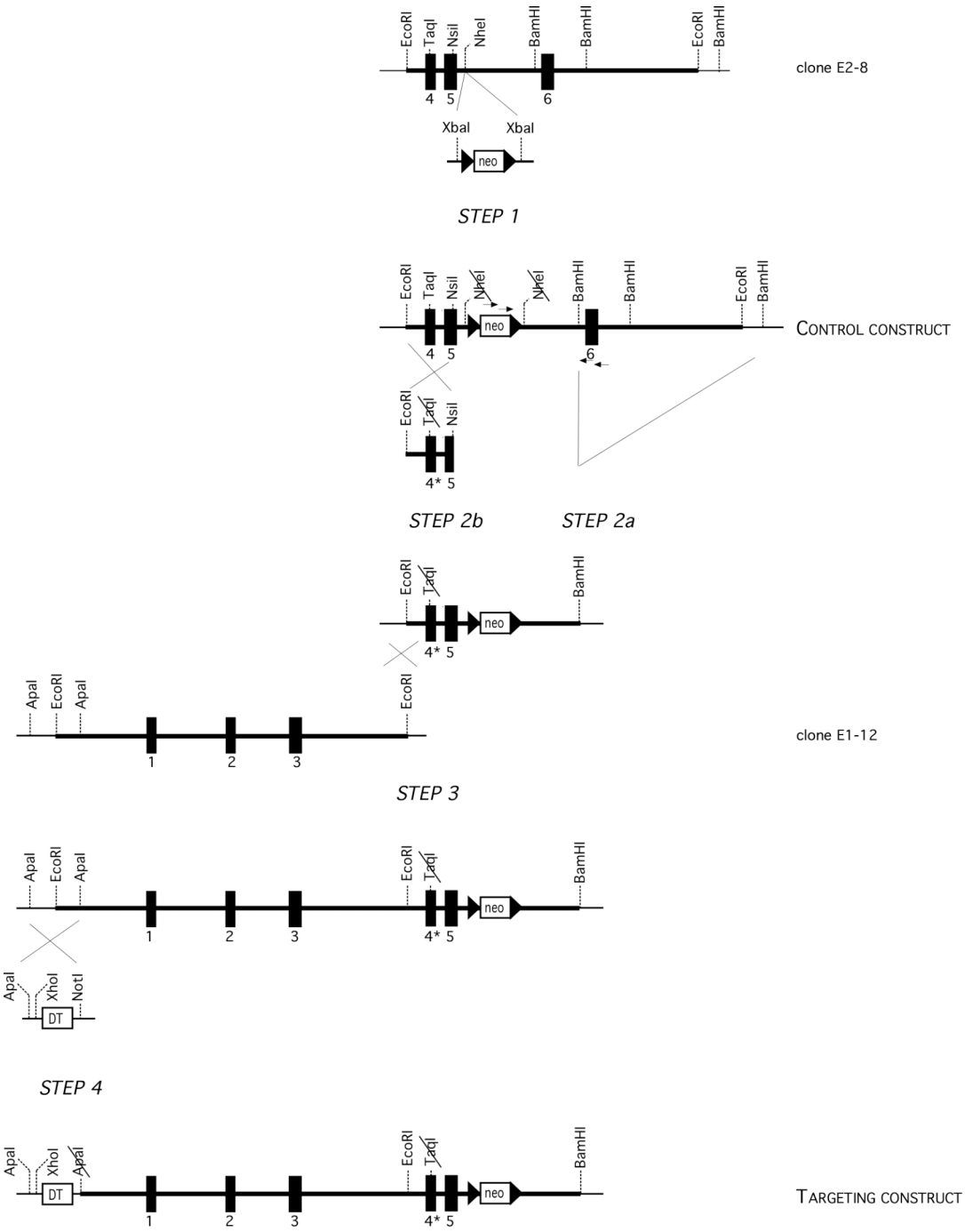

Figure 8 Construction of R91W targeting vector

STEP 1; Incorporation of the floxed Neo cassette into clone E2-8 resulting in creation of the control construct used to establish the PCR conditions to detect the HR event. Arrows in the control construct represent the positions of the two nested primer pairs used. STEP 2a; truncation of the 3' region of the control construct to create the short arm of the targeting construct suitable for screening of a HR event by PCR. STEP 2b; introduction of the R91W mutation contained in the EcoRI/NsiI (525 bp) fragment (see Figure 7C). STEP 3; addition of the 5' region contained in clone E1-12 (exons 1-3) to create the long arm of the construct. STEP4: Incorporation of the diphteria toxin (DT) cassette as negative selection marker at the 5’ end resulting in creation of the final targeting construct. The positions of the most relevant restriction

enzyme sites are indicated. The unique XhoI restriction site was used for linearization of the vector prior to electroporation into ES cells.

2.1.5 Electroporation of embryonic stem (ES) cells

The XhoI-linearized control, targeting or unrelated vector were electroporated into isogenic TC-1 embryonic stem (ES) cells derived from 129Sv mice (Deng et al. 1995; Katschinski et al. 2003). For this purpose 30 µg of vector and $5x10^6$ TC- ES cells were pulsed at 240 V / 500 µF (Bio-Rad Gene Pulser, Reinach, Switzerland). After 48 hours of recovery, selective media containing 200 µg/ml G418 (Calbiochem, La Jolla, Calif.) was added to the ES cells for additional 8 days. 10 days following electroporation G418-resistant colonies were picked. Genomic DNA from G418-resistant ES clones was analyzed for correct vector integration by PCR and Southern blotting as described in section 2.1.6.

2.1.6 Assessing the ES cells for homologous recombination

To establish the PCR conditions for detection of HR event, ES cells were electroporated with control construct carrying the neo gene (Figure 8) and with a unrelated construct and cultured as described in section 2.1.5. Single G-418 resistant colonies were picked and one colony transfected with the control construct was pooled with 7 or 11 unrelated transfected ES colonies to test for PCR sensitivity. Genomic DNA was isolated and PCR conditions were tested.

For the detection of the correctly integrated neo cassette, two primer pairs have been selected to allow a nested PCR approach (Figure 9B; Table 2). For the neo1 primer pair the forward primer was designed within the neo cassette and the reverse primer was positioned outside of the targeted DNA sequence (Figure 9B; Table 2). To further minimize any false positive result, a nested neo2 primer pair was created within the same area, thus only correctly integrated DNA should be detectable by PCR (Figure 9B; Table 2). A Taq primer pair was used to detect the presence of the R91W mutation. This pair produced a 998 bp fragment from both, wild-type and mutant DNA. Only the wild-type DNA amplicon included a TaqI restriction site, resulting in 619 and 379 bp fragments after incubation with TaqI restriction enzyme.

DNA from G418-resistant ES cells was analyzed by Southern blotting. An external 3' BamHI probe (759-bp) was random-labeled using the DIG labeling kit

(#1585614, Roche Diagnostics, Mannheim, Germany). Genomic ES cell DNA was digested overnight with EcoRI and electrophoresed on a 0.8% agarose gel. DNA samples were transferred onto a nylon membrane by a capillary method. The membrane was incubated with the DIG-labelled probe. Fragments corresponding to wild-type and knock-in alleles (5.6 and 7.7 kb, respectively) were detected by enhanced chemiluminescence (Figure 9B).

2.1.7 Blastocyst injection, assessment of germ line transmission and crossbreeding

10-20 positive ES clones, containing a homologously recombined R91W mutation, were injected into blastocyst originating from C57BL/6 mice. 10 blastocysts per uterus were transferred into foster NMRI mothers. 2 chimeric males were born. Germ line transmission was tested by breeding the chimeric males with C57BL/6 females and positive selection was performed by coat color assessment (agouti color was expected for positive offspring) and PCR genotyping using neo1, neo2 and TaqI primer pairs (section 2.1.6, Table 2 and Figure 9B).

Table 2 PCR primers used for genotyping of different mouse strains

Primer name	*Forward (5'-3')*	*Reverse (5'-3')*	*Product Size (bp)*
neo1*	AGCAGCCTCTGTTCCACATAC	GATGAGCAGTGGCACCATTG	1513
neo2*	CTCAGTATTGTTTTGCCAAG	GATCAACCTGTAGAATGAAAG	1445
Cre*	GGACATGTTCAGGGATCGCCAGGCG	GCATAACCAGTGAAACAGCATTGCTG	268
Taq*	GCTGGTCTTGCCTGTATCA	GTCAGAGACAGTGCTGTGTT	998
***Rpe65**$^{-/-}$*	GATGTGGGCCAGGGCTCTTTGAAG	GGGAACTTCCTGACTAGGGGAGG	459
***Rpe65**$^{+/+}$*	GATGTGGGCCAGGGCTCTTTGAAG	CCCAATAGTCTAGTAATCACAGATG	546
***Rho**$^{-/-}$*	TCTCTCATGAGCCTAAAGCT	TTCAAGCCCAAGCTTTCGCG	310
***Rho**$^{+/+}$*	TCTCTCATGAGCCTAAAGCT	ATGCCTGGAACCAATCCGAG	470

*primers related to the generation of R91W knock-in mice

** Taq primer pair used to genotype R91W mice. Genotyping included digestion of the 998 bp PCR product by TaqI restriction. This digestion results in generation of 619 and 379 bp fragments in wild-type animals, or no cleavage in R91W knock-in animals.

*$^{+}$The genotyping using neo1 and neo2 included: a first PCR using the neo1 primer pair amplified for 20 cycles followed by the nested PCR using neo2 primer pair amplified for 35 cycles.

Primers for genotyping the Rpe65 and Rho mice are as previously described (Humphries et al. 1997; Redmond and Hamel 2000)

Following the confirmation of germ line transmission, the chimeric male was bread to 129S6 females to propagate the line on a co-isogenic background. This breeding resulted in the generation of a heterozygous Rpe65^{R91Wneo} line. The genotype was confirmed by PCR using neo1, neo2 and TaqI primer pairs.

For *in vivo* removal of the neo resistance cassette, Rpe65^{R91Wneo} mice were bred with deleter mice expressing cre recombinase in their germ line (129S6-TgN(Prnp-GFP/Cre)1Blw/J (Scheel et al. 2003)). The Rpe65^{R91Wneo} mice were kept on a cre-deleter background for 2 generations to ensure complete excision of the floxed-neo cassette. The deletion of the neo cassette was confirmed by PCR genotyping using neo1, neo2 and cre primer pairs (see Table 2). Finally, the resulting heterozygous R91W/wt offspring was intercrossed to obtain R91W homozygous mice. The genotyping of the final R91W knock-in mice was preformed by PCR on tail genomic DNA using the TaqI primer pair as described in Table 2.

2.2 Animals

All procedures concerning animals were in accordance with the regulations of the Veterinary Authority of Zurich and with the statement of 'The Association for Research in Vision and Ophthalmology' for the use of animals in research. All animals were raised in cyclic light (12:12 h; 60 lux at cage level). The cre expressing mice 129S6-TgN(Prnp-GFP/Cre)1Blw/J (Scheel et al. 2003) and corresponding wild-type mice (129S6) were purchased from the Jackson Laboratory (Bar Harbor, USA). Rhodopsin deficient mice (Rho$^{-/-}$) were generously provided by M. Seeeliger (University Eye Hospital, Tuebingen, Germany)(Humphries et al. 1997). Rpe65 deficient mice (Rpe65$^{-/-}$) were maintained at the University Hospital Zurich (Redmond et al. 1998). The double mutant R91W;Rho$^{-/-}$ and Rpe65$^{-/-}$;Rho$^{-/-}$ mice were generated by classical breeding schemes. Genotyping was performed by PCR on tail genomic DNA, using the primers shown in Table 2.

2.3 RNA isolation, reverse transcription and quantitative real-time PCR

Retinas were removed through a slit in the cornea. The remnant eyecup tissue containing RPE was isolated separately. The isolated tissue was immediately frozen in liquid nitrogen and stored at -70 °C until RNA preparation. RNA was isolated using RNeasy Mini Kit (Qiagen, Hilden, Germany) following the manufacturer's protocol. Briefly, a retina was homogenized in 350 µl lysis buffer containing β-mercaptoethanol by using a syringe and passing the lysates 10 times trough a 21-G needle. After addition of 70% ethanol, the lysate was applied to the RNA-binding column. To minimize DNA contamination, nucleic acids bound to the membrane were treated with DNase. After several steps of washing, RNA was eluted with 50 µl of RNase-free water and its concentration was measured by spectrophotometry.

For reverse transcription (RT) typically 650 ng of RNA was used. RT-PCR was carried out by using oligo dT and M-MLV reverse transcriptase (Promega, Madison, USA) in a final volume of 25 µl. The RT was performed at 37°C for 1.5 h, followed by incubation at 65°C for 10 min. cDNA corresponding to 10 ng of total RNA was amplified with specific primers in subsequent PCR reactions (Table 3).

Table 3 Primers and PCR conditions used for quantitative gene expression analysis

Gene	*Forward primer (5'-3')*	*Reverse primer (5'-3')*	*Ann. temp.(°C)*	*Elong. time (s)*	*Size (bp)*
β-actin	CAACGGCTCCGGCATGTGC	CTCTTGCTCTGGGCCTCG	58	7	153
SWL opsin*	TGTACATGGTCAACAATCGGA	ACACCATCTCCAGAATGCAAG	58	7	153
MWL opsin*	CTCTGCTACCTCCAAGTGTGG	AAGTATAGGGTCCCCAGCAGA	58	7	154
Rod opsin	TTTTATGTGCCCTTCTCCAACG	ATGATAGCGTGATTCTCCCCG	60	19	440
GNAT1*	GAGGATGCTGAGAAGGATGC	TGAATGTTGAGCGTGGTCAT	58	9	209
GNAT2*	GCATCAGTGCTGAGGACAAA	CTAGGCACTCTTCGGGTGAG	58	8	192
Rpe65 **	ATGACTGAGAAGAGGATTGTC	CTGCTTTCAGTGGAGGGATC	60	15	366
MCT3	GGCTCAACCCTAAATCCAGA	CTTCGGAGTTTCCTCACCAG	58	4	75
FGF2	TGTGTCTATCAAGGGAGTGTGTGC	ACCAACTGGAGTATTTCCGTGACCG	62	7	158
GFAP	CCACCAAACTGGCTGATGTCTAC	TTCTCTCCAAATCCACACGAGC	62	10	240
Casp-1	GGCAGGAATTCTGGAGCTTCAA	GTCAGTCCTGGAAATGTGCC	60	6	138

* primers described in(Znoiko et al. 2005); ** primers described in (Redmond et al. 1998)

cDNA quantification was carried out by real-time RT-PCR using either SYBR Green JumpStart Taq ReadyMix kit (Sigma, Saint Louis, USA) or the LightCycler 480 Sybr Green I Master kit (Roche, Mannheim, Germany). Amplifications were performed using a Light Cycler instrument (Roche, Mannheim, Germany). The PCR included a hot start denaturation at 95 °C for 10 minutes, followed by 45 cycles, with melting at 95 °C for 5 seconds, annealing for 8 seconds and elongation at 72 °C (annealing temperatures and elongation times indicated in the Table 3). Melting curve analysis was performed (0.1 °C/sec increase from 65 °C to 95 °C, with continuous fluorescence readings) at the end of 45 cycles, to control for the specificity of the reaction. For the relative quantification of gene expression, mRNA levels were normalized to β-actin for retinal samples or to MCT3 (monocarboxylic acid transporter 3) for eyecups using the ΔΔCT (comparative threshold cycle) method. Relative values were calculated using a respective calibrator sample as indicated in the results. Each reaction was run in triplicates.

2.4 Western blotting

The isolation of retinal and eyecup proteins was as follows: the eye was enucleated and lens and vitreous were removed through a slit in the cornea. The retina was separated from eyecup and tissues were separately homogenized in Tris buffer (0.1 M, pH 8.0) using an ultrasound tip at 4 ^{o}C. The homogenate was centrifuged for 1 min at 1000 x g, the supernatant was analyzed for its protein content (Bradford Assay, Bio-Rad), mixed with SDS sample buffer, and heated for 10 min at 70 ^{o}C.

The isolated proteins were subjected to SDS-PAGE and blotted onto nitrocellulose. The membranes were probed with primary antibodies, followed by horseradish peroxidase-conjugated secondary antibodies. The primary antibodies used were: rabbit anti-Rpe65 (pin5; 1:2'000); rabbit anti-RGR (pin3; 1:5'000); mouse anti-LRAT (1:1'000; gift from K. Palczewski University of Washington, Seattle, USA); rabbit anti-Cralbp (UW55; 1:10'000, gift from J. C. Saari, University of Washington, Seattle, USA). Protein bands were visualized with the addition of an enhanced chemiluminescent substrate (PerkinElmer, Boston, USA) and exposure to Super RX film (Fujifilm, Dielsdorf, Switzerland). At least three animals were analyzed per condition and genotype. Quantification of RPE65 immunoreactivity was done using anti-rabbit secondary antibodies conjugated to IR dye 800 (Rockland

Immunochemicals) and quantified using the Odyssey infrared imaging system (LI-COR Biotechnology, Cambridge, UK) with β-actin as standard (Santa Cruz, USA).

2.5 Rhodopsin measurements

Rhodopsin content was analyzed as described earlier (Wenzel et al. 2005). The mice were dark adapted for 24 h, sacrificed under dim-red light and retinas - isolated through a slit in the cornea - were placed in 1 ml of distilled H_2O. After 10 min of centrifugation at 15'000 x g, the pellet was mixed with 700 µl of 1% hexadecyltrimethylammonium bromide (Fluka Chemie, Buchs, Switzerland) and homogenized with a Polytron for 10 sec. The homogenate was centrifuged for 10 min at 15'000 x g, and the supernatant was collected. The absorption at 500 nm was measured before and after exposure to bright white light (20,000 lux for 1 min). The amount of rhodopsin present per retina was calculated using the following formula derived from the Lambert-Beer equation: $rho = V \times c = V \times \Delta A_{500} / (\varepsilon_{500} \times l \times n)$. rho is the amount of rhodopsin per retina [mol]; V, the volume of sample [l]; c, the concentration of rhodopsin per retina [M]; ΔA_{500} is the difference between absorption before and after bleaching measured at 500 nm; ε_{500}, the extinction coefficient of rhodopsin at 500 nm [4.2×10^4 $M^{-1}cm^{-1}$]; l, the path length of the cuvette [cm]; and n is the number of retinas. At least three animals were analyzed per condition and genotype.

2.6 Rhodopsin regeneration kinetics

The kinetics of rhodopsin regeneration after bleaching was analyzed in mice that were dark adapted for 24 hours. 30-60 min prior to light exposure, pupils were dilated (Cyclogyl 1%; Alcon, Cham, Switzerland; and phenylephrine 5%, Ciba Vision, Niederwangen, Switzerland) under dim red light (≥650 nm). Animals were exposed for 10 min to 5'000 lux of fluorescent white light (TLD-36 W/965 tubes; Philips, Hamburg, Germany; UV-impermeable diffuser). Following illumination mice were placed in darkness for the times indicated in the results and rhodopsin content was analyzed as described above. Non-exposed mice served as dark-controls. At least three animals were analyzed per condition and genotype.

2.7 Histology

Animals were sacrificed and the superior portion of the eye was marked. The enucleated eyes were fixed in 2.5% glutaraldehyde prepared in 0.1 M cacodylate buffer. After overnight fixation, the cornea, lens and vitreous were removed and superior part of the eye was separated from inferior by a cut through the optic nerve head. The tissue was washed in 0.1 M cacodylate buffer two times for 15 min, postfixed in 1% osmiumtetroxid for 1 hour, and dehydrated in ethanol series (30% 5 min, 50% 15 min, 70% 15 min, 96% 15 min, 100% 3 x 15 min). The tissue was incubated in propylenoxid (2 x 15 min), propylenoxid/Epon 812 mix (1:1, 3 h), followed by pure Epon (overnight). The next day tissue was embedded in Epon with addition of N-benzyl-dimethylamin as catalyzer of polymerization and incubated at 60 ^{o}C for 2 days. For light microscopy, 0.5 μm thin sections were prepared from the inferior central retina, counterstained with methylene blue, and analyzed using a microscope (Axiovision, Zeiss, Germany). For electron microscopy, sections (50-60 nm) were contrasted with 4% uranyl acetate in 50% EtOH and 2.6% lead nitrate in 1 M NaOH. Sections were analyzed using a Hitachi 7000 electron microscope (Hitachi, Tokyo, Japan).

2.8 Immunofluorescence

Animals were sacrificed and the superior part of the eye was marked for orientation. The enucleated eyes were immersed in cryoprotective medium (Jung, Nussloch, Germany), frozen in liquid nitrogen and stored at -70 ^{o}C until further use. 10-20 µm sections were cut temporal to nasal trough the optic nerve head. Sections were dried overnight at room temperature, fixed in cold acetone for 10 min, washed in PBST (PBS + 0.05% Triton X-100) for 2 x 5min at room temperature (RT). After blocking in PBST containing 10% normal goat serum (NGS) for 1h at RT, sections were incubated with the anti-rabbit RPE65 primary antibody (1:500) in PBST containing 3% NGS at 4 ^{o}C, overnight. Sections were washed 3 x 10min in PBST and secondary antibodies (Cy3 conjugated; Jackson ImmunoResesarch, Soham, UK) were applied in PBST containing 3% NGS for 1-2h at RT. Sections were washed 2 x 10min in PBST and 1 x in PBS and rinsed in water before they were covered with PBS containing 75% glycerol and 30 mg/ml diazo-bicyclo-octane. Immunofluorescence was analyzed on a microscope (Axiovision, Zeiss) and documented using a digital imaging system.

2.9 Cone quantification

For cone quantification, eyes were marked nasally, enucleated and perforated at the cornea to allow better penetration of the fixative. After fixation for 1h in 4% PFA (in PBS) the eyes were cryoprotected in 25% sucrose solution. The eyes were embedded in albumin from hen egg white (Fluka, Buchs, Switzerland) and cut dorsal to ventral trough the optic nerve head. 14 µm sections slides were blocked for at least 1h at room temperature in PBS containing 0.2% Triton and 10% NGS (Dako, Zug, Switzerland) or 10% normal horse serum (NHS) (Jackson Immunoresearch). The primary and secondary antibodies were incubated in PBS containing 0.2% Triton and 2% NGS or 2% NHS.

Rabbit anti-GNAT2 (Santa Cruz, USA) was incubated overnight at room temperature at 1:100; goat anti-SWL-opsin (Santa Cruz, USA) and rabbit anti-MWL (Chemicon, Temecula, CA, USA) overnight at 4ºC at 1:1000. Secondary antibodies goat anti-rabbit linked to FITC (1:100, Jackson Immunoresearch, Westgrove, PA, USA) or Cy3 (1:500, Jackson Immunoresearch) were incubated 1 hour at room temperature. For immunolabelling of the anti-SWL-opsin, donkey anti-goat-Cy3 (1:1000, Jackson Immunoresearch) was used. Before examination, sections were counterstained with 4',6-diamidino-2-phenylindole dilactate (DAPI, Molecular Probes) and mounted with Mowiol 4-88 Reagent (VWR International AG, Lucerne, Switzerland).

The sections trough the optic nerve e.g. the most transversal ones were chosen to quantify the number of cells positive for GNAT2, MWL and SWL-cone opsins, respectively. The immunoreactive outer segments were counted from periphery to periphery using a BX60 microscope equipped for epifluorescence (Olympus Suisse SA, Aigle, Switzerland) and coupled to the analySIS® 3.0 software (Soft Imaging System). At least 4 eyes per condition and genotype were analyzed.

2.10 HPLC determination of retinoids

HPLC profiling of retinoids was performed in mice dark adapted for 24 hours. All steps were carried out under dim red light. Animals were sacrificed, lens and vitreous were removed from the eye through a slit in cornea. The rest of the tissue containing retina and eyecup was snap frozen in liquid nitrogen until further analysis.

The tissue was transferred into 200 µl of 2 M NH_2OH (pH 6.8) (results in formation of retinaloximes) and 200 µl of methanol and was homogenized by sonification (5 bursts for 5 s, 20% of maximum power, Sonoplus, Bandelin, Berlin, Germany), followed by incubation for 10 min at RT. Then, 400 µl acetone were added. Extraction was performed three times with 500 µl petroleum ether each. The collected organic phases were dried on speedvac and dissolved in the HPLC solvent (n-hexane/ethanol, 99.5:05). HPLC analyses was performed on a Hypersil 3 µm (Knaur, Germany) on a System Gold (Beckman Instrument, Fullerton, USA) equipped with a multidiode array (model 166, Beckman) and the System Gold Nouveau software (Beckman). The reference substances all-*trans*, 13-*cis*, and 9-*cis* retinal were purchased from Sigma (Sigma, Saint Louis, USA); 11-*cis* retinal was isolated from dark-adapted bovine eyes. The corresponding retinols and oximes were obtained by reducing with $NaBH_4$ or reaction with NH_2OH, respectively. For quantification of the molar amounts, peak integrals were scaled with defined amounts of reference substances. Peak integrals were calculated using the 32 Karat software (Beckman).

2.11 ERG functional tests

The ERGs were performed according to previously described procedures (Seeliger et al. 2001). Briefly, mice were dark-adapted overnight before the experiments. Anesthesia was induced by subcutaneous injection of ketamine (66.7 mg/kg) and xylazine (11.7 mg/kg). Silver needle electrodes served as reference (forehead) and ground (tail) electrodes, and gold-wire ring electrodes as active electrodes. The ERG equipment consisted of a Ganzfeld bowl, a DC amplifier, and a PC-based control and recording unit (Toennies Multiliner Vision; Jaeger/Toennies, Höchberg, Germany). The pupils were dilated and single white-flash recordings were obtained from both dark-adapted (scotopic) and light-adapted (photopic) conditions.

Light adaptation was accomplished with a background illumination of 30 cd/m^2 starting 10 minutes before recording. Single white-flash stimulation ranged from -4 log candelas*second per m^2 (cd*s/m^2) to 1.5 log cd*s/m^2 under the scotopic condition, and from -2 to 4 log cd*s/m^2 under the photopic condition, divided into 10 (scotopic) and 13 (photopic) steps of 0.5 and 1 log cd*s/m^2. Responses were averaged with an inter-stimulus interval (ISI) of either 5 seconds or 17 seconds (for above 0 log cd*s/m^2). At least 3 animals were analyzed per genotype and age.

3 RESULTS

3.1 Generation of R91W knock-in mice

Gene targeting in mouse ES cells was used to modify exon 4 of the Rpe65 gene such that codon 91 changed from arginine to tryptophan (R91W) (Figure 9A). In humans, the R91W mutation is caused by a single point mutation (TGA>TGG). However, mouse arginine 91 is encoded by CGA codon, therefore two point mutations had to be introduced into codon 91 (CGA>TGG). The introduction of these two mutations resulted in the loss of a TaqI restriction site, facilitating the genotype analysis (Figure 9A, B).

The gene targeting strategy is shown in Figure 9B. In addition to mouse Rpe65 genomic DNA carrying the R91W mutation, the targeting vector contained a floxed neomycin resistance (neo) and a diphtheria toxin (DT) cassette as selection markers. Sequencing of the full genomic DNA insert of the targeting vector confirmed the presence of the R91W mutation and the selection markers in an otherwise wild-type sequence. After electroporation and selection on G418 medium, positive ES cells were identified and characterized in detail by Southern blotting, PCR and PCR restriction digestion analysis (Figure 9C and data not shown).

Correctly targeted ES clones were used to generate germ line competent chimeric mice. A chimeric male was mated to isogenic 129S6 females to propagate the line. The resulting heterozygous ($Rpe65^{R91Wneo}$) F1 mice were bred with a germ line Cre-deleter mouse line (129S6-TgN(Prnp-GFP/Cre)1Blw) (Scheel et al. 2003) to excise the neo cassette (Figure 9B). The resulting offspring was heterozygous for the R91W mutation (R91W/wt), and the only foreign sequence remaining was a single loxP site. Finally, we interbred the heterozygous (R91W/wt) mice to obtain pure R91W mice. Of note, these mice were isogenic to 129S6 control mice, except for codon 91 and the above mentioned loxP site.

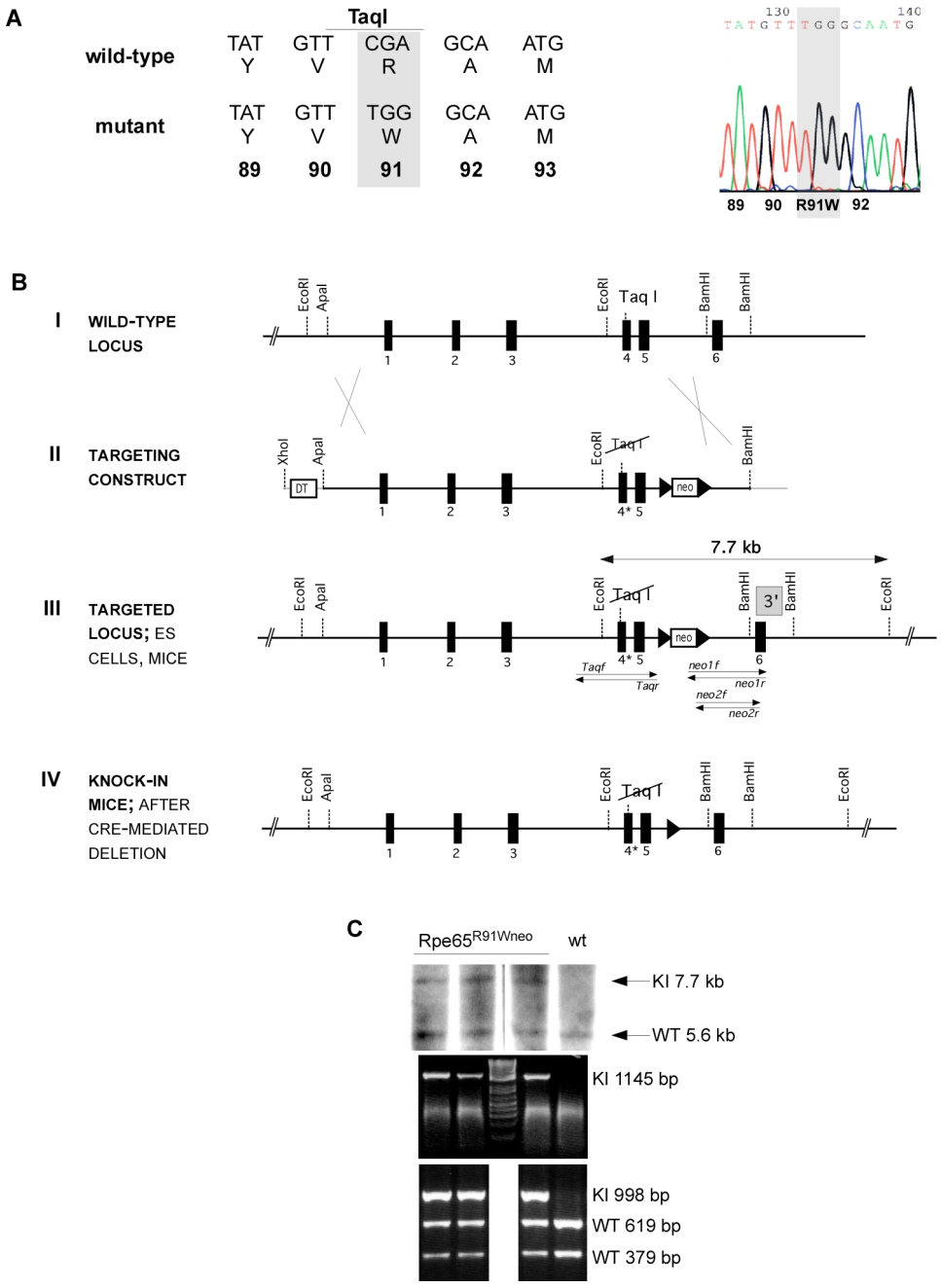

Figure 9 Generation of R91W knock-in mice

A, Partial sequence of exon 4 wild-type and mutated R91W DNA. Note that two point mutations were introduced in the codon for arginine (R) at position 91 to obtain tryptophan (W). This resulted in loss of a TaqI restriction site in the mutated DNA (right panel). Sequence data of the targeting vector showing a mutant TGG triplet at position 91 (right panel).

B, Schematic representation of the R91W targeting strategy

I: Partial wild-type Rpe65 allele, with restriction enzyme sites and location of exons (boxes). The restriction sites given were used to analyze particular steps in cloning of the targeting vector (see method section).

II: Targeting construct containing R91W mutation (indicated as lost TaqI restriction site in exon 4), neomycin resistant gene flanked by loxP sites (indicated as triangles) suitable for cre-medated excision, and diphtheria resistance cassette (DT). Note the unique XhoI restriction site used for linearization of the targeting vector.
III: Mutated genomic Rpe65 DNA after HR selection containing the neomycin cassette ($Rpe65^{R91Wneo}$). The targeted locus with depicted positions of primers and probes for PCR and Southern blot analyses. Neo1 and neo2 are nested primer pairs designed to read from the selection cassette into the 3' short arm outside of targeting area. These primers were used to confirm the homologous recombination. The Taq primer pair was used to confirm the presence of R91W mutation (see methods).
IV: The partial R91W mutant allele after the removal of the neo cassette by crossing $Rpe65^{R91Wneo}$ mice with the Cre-deleter mice.

C, Genotyping of R91W mutants.
Upper panel: DNA was isolated from neomycin-resistant ES cell colonies, and analyzed by Southern blotting, after digestion by EcoRI, and using 3'external probe as indicated in Figure 9B. Signal from the genomic DNA from wild-type (wt) allele is 5.6 kb. A heterozygous $Rpe65^{R91Wneo}$ knock-in (KI) allele gives rise to additional 7.7 kb due to the presence of neomycin cassette.
Middle panel: PCR analysis of the same DNA using neo1 and neo2 nested primer pair. A PCR fragment of 1145 bps detected in heterozygous $Rpe65^{R91Wneo}$ knock-in due to the presence of the neomycin cassette.
Lower panel: RFLP-PCR analysis of the same DNA using the Taq primer pair (see Figure 9B). A PCR fragment of 998 bps was digested with the TaqI restriction enzyme. In wild-type animals this results in a 379 and a 619 bp fragments. Heterozygous $Rpe65^{R91Wneo}$ knock-in DNA contains an additional 998 bp fragment due to the loss of the TaqI restriction site. This protocol was used for genotyping of the final R91W knock-in mice.

3.2 Rpe65 expression in the mutant mice

In order to test whether R91W knock-in mice express RPE65, we analyzed its expression by quantitative RT-PCR, Western blotting and immunohistochemistry (Figure 10A, B and C). While the expression of Rpe65 mRNA was relatively slightly reduced in R91W mice (Figure 10A), Western blotting revealed that the steady state levels of the mutant protein were reduced by 95% (not shown) as compared to wild-type control (Figure 10B). Nevertheless, the mutant protein was correctly localized to the RPE as described for wild-type mice (Seeliger et al. 2001; Hemati et al. 2005). No RPE65 expression could be detected in control experiments using RNA (RT-PCR), protein extracts (Western blotting) or tissue (immunohistochemistry) from RPE65 deficient mice (Figure 10A, B and C).

We also compared the amount of several proteins (retinal G protein coupled receptor, RGR; lecithin retinol acyltransferase, LRAT; and cellular retinaldehyde binding protein, CRALBP) that are involved in retinoid recycling and may at least functionally be connected to RPE65 (Saari 2000; Van Hooser et al. 2002; Wenzel et al. 2005). In eyecups of 8 week-old age-matched wild-type, R91W knock-in and $Rpe65^{-/-}$ animals the expression levels of these three proteins were similar with a tendency of increased LRAT levels in mutant mice (Figure 10B).

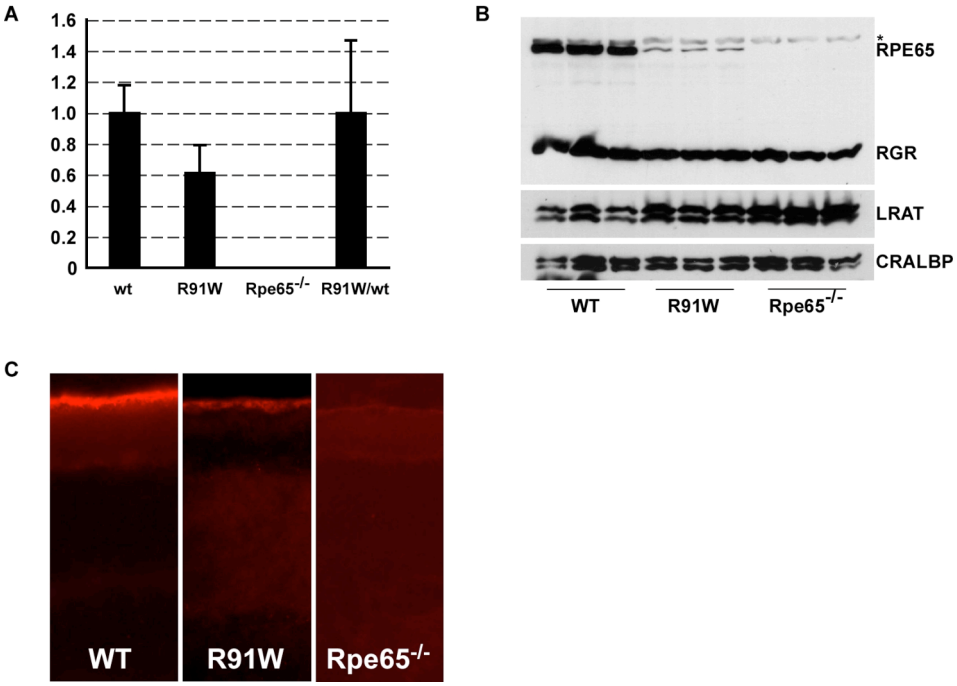

Figure 10 R91W mutation causes reduced levels of RPE65

A, Relative mRNA levels of Rpe65 expressed in eyecups of wild-type, R91W, Rpe65$^{-/-}$ and R91W/wt mice at 8 weeks of age as determined by real-time RT-PCR. mRNA levels are expressed relative to wild-type control, which was set to 1. RNA isolated from 3 independent retinas per age and genotype was amplified in triplicates (means ± S.D.).

B, Western blotting of eyecup proteins from three animals of each genotype (wild-type, R91W and Rpe65$^{-/-}$ mice) are shown. Presence of the R91W mutation resulted in reduced amounts of RPE65 immunoreactivity but had clearly less effects on the protein levels of RGR, LRAT and CRALBP.
*, unspecific band.

C, Immunolabeling with a polyclonal antibody to RPE65, demonstrating that the R91W mutant protein is expressed in RPE cells only. Note the reduced immunoreactivity as compared to animals expressing wild-type RPE65 protein. The Rpe65$^{-/-}$ animals served as negative controls and no staining was observed in their RPE.

3.3 Retinoid analysis

The absence of RPE65 in mice results in the arrest of the visual cycle causing accumulation of retinyl esters in the RPE and lack of rhodopsin (Redmond et al. 1998). In line with this observation, dramatically reduced protein levels of mutant RPE65 (Figure 10B) pointed to a similar disturbance of the visual cycle of R91W mice. Therefore, we analyzed the retinoid profile in wild-type, R91W/wt heterozygous, R91W homozygous and Rpe65$^{-/-}$ mice at different ages.

The analysis of combined retina and eyecup preparations (see methods section) of 4, 8, 12, 24 and 40 week-old animals revealed highly reduced levels of 11-*cis* retinal in R91W homozygous mice, suggesting strong influence of the mutation on the visual cycle (Table 4). However, clear differences between Rpe65$^{-/-}$ and R91W mice were observed: While 11-*cis* retinal was not detectable in Rpe65$^{-/-}$ mice at any age, retinas from R91W knock-in mice contained between 9.4 and 24 pmol of 11-*cis* retinal (Table 4). These numbers represent between 2.5% and 6.3% of the levels found in age-matched wild-type animals.

Table 4 Retinoid analysis

GENOTYPE	AGE	*11-cis* retinal	*All-trans* retinal	*All-trans* retinol	Retinyl ester	9-*cis* retinal
wild-type	4	380.2±60.1	39.0±11.3	4.2±3.6	30.6±5.6	0
	8	336.1±21.8	34.7±1.6	5.4±9.4	39.2±5.0	0
	12	336.7±32.4	62.6±12.9	0	34.9±4.6	0
	24	373.6±75.5	47.9±3.7	2.2±3.8	106.2±27.2	0
R91W/wt	4	394.7±22.6	53.4±7.1	6.0±0.8	44.3±5.4	0
	8	371.8±22.1	87.1±4.7	0	55.7±8.4	3.7±0.3
	12	454.8±42.0	52.4±5.5	3.0±3.7	89.6±17.9	0
	24	337.4±49.0	86.4±15.3	0	108.9±23.3	0
R91W	4	24.0±3.0	3.6±0.6	10.4±1.9	420.7±34.5	7.6±0.8
	8	15.4±0.2	4.8±1.5	9.2±5.2	651.9±127.4	9.9±0.9
	12	13.5±0.2	2.7±0.4	13.9±2.7	1542.7±271.8	9.2±1.2
	24	9.4±8.2	1.9±1.7	20.2±17.7	2186.1±160.1	4.3±3.7
	40	18.2±4.8	2.2±1.0	12.4±3.4	2107.9±138.9	10.6±3.2
Rpe65$^{-/-}$	4	0	0	8.6±2.5	271.4±22.8	4.8±1.5
	8	0	1.3±1.2	5.4±1.0	474.9±49.1	8.5±0.7
	12	0	1.9±0.4	14.9±4.1	805.9±57.5	6.7±0.9
	24	0	2.1±0.3	8.5±4.8	1160.6±529.0	10.3±3.8
	40	0	2.8±1.0	15.6±5.1	2622.9±531.3	13.1±11.2

All values are given in pmol/eye ±S.D. (n=3).

The presence of reduced amounts of 11-*cis* retinal in R91W animals indicated that the visual cycle is affected but nevertheless might be functional. In addition, we

detected a strong accumulation of retinyl esters in the R91W knock-in animals. The initial rate of retinyl esters accumulation during the first 24 weeks was almost linear (13 pmol/day; R^2=0.93). By the end of this period, retinyl esters seemed to reach maximal levels in R91W mice, as there was no difference between 24 and 40 week containing 2186 and 2108 pmol/eye, respectively. In Rpe65$^{-/-}$ animals linear accumulation of retinyl esters was detected trough all tested time points (9 pmol/day; R^2=0.96) and the highest levels detected were 2623 pmol/eye in 40 week-old animals. All-*trans* retinal, all-*trans* retinol and 9-*cis* retinal levels were comparable in both R91W and Rpe65$^{-/-}$ mice. The retinoid content was comparable between wild-type and R91W/wt heterozygous animals at all tested time points (Table 4).

In Rpe65$^{-/-}$ mice, the over-accumulation of retinyl esters results in formation of microscopically visible lipid inclusions in the RPE (Redmond et al. 1998). Because R91W mice showed increased levels of retinyl esters we analyzed the RPE of 8 week-old animals of all 4 genotypes by electron microscopy (Figure 11). Unlike in wild-type and heterozygous animals, the electron microscopy revealed the presence of numerous lipid droplets in RPE of both Rpe65$^{-/-}$ and R91W mice.

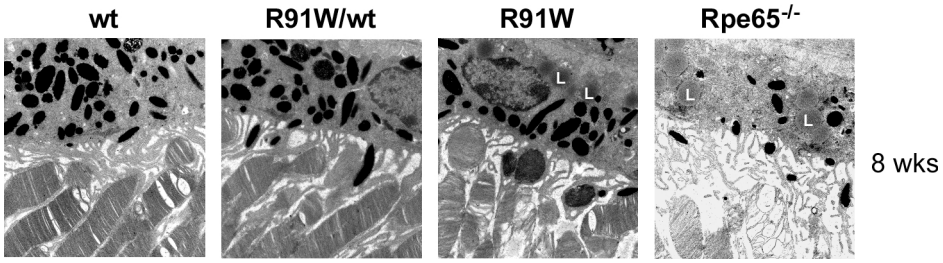

Figure 11 Lipid-like inclusions in R91W mice

Electron microscopy of the RPE-photoreceptor interface in 8 week-old wild-type, R91W/wt heterozygous, R91W homozygous and Rpe65$^{-/-}$ mice. Note that lipid-like inclusions ("L") and disturbed outer segment morphology are present in R91W and Rpe65$^{-/-}$ mice only.

3.4 Rhodopsin content and regeneration

11-*cis* retinal levels measured in dark-adapted 4 week-old R91W mice corresponded to approximately 6% of wild-type levels (Table 4). Likewise, the rhodopsin levels in R91W mice, which were dark-adapted for 24 h, were 30 pmol/retina or 6% of wild-type rhodopsin levels (Figure 12A).

The kinetics of rhodopsin regeneration is governed by the expression levels of Rpe65 protein (Wenzel et al. 2003; Lyubarsky et al. 2005). Given that lower amounts of RPE65 were detected in the RPE of R91W mice (see Figure 10), we expected that rhodopsin would regenerate with a slower rate in these animals. To allow for a complete regeneration of rhodopsin without daily bleaching, we kept R91W mice in darkness for 4, 10 and 22 days. By the time of analysis the mice were 6-7 week-old. However, even prolonged dark adaptation did not raise rhodopsin levels significantly. Maximal rhodopsin levels detected after 22 days in darkness were 42 pmol, which was still less than 10% of the rhodopsin content detected in wild-type animals (Figure 12A, see Figure 12C for the wild-type levels).

In order to test rhodopsin regeneration kinetics following a strong bleach, 6-7 week-old animals were dark-adapted for 24h and exposed for 10 min to 5000 lux, which induces 90% bleach in wild-type animals (Wenzel et al. 2005), and returned back to darkness until analysis. Non-exposed R91W mice contained 27 pmol of rhodopsin (Figure 12B). Retinas of animals analyzed immediately following the exposure contained 1 pmol of rhodopsin. However, even after 5 days of recovery in darkness only 44% (12 pmol) of the dark-adapted rhodopsin levels (27 pmol) were detectable. Thus, following a strong bleach, regeneration of rhodopsin was unexpectedly inefficient and reached a plateau at about half the maximal level.

Maximal rhodopsin levels were similar in R91W/wt heterozygous and wild-type animals; 538 pmol/retina and 560 pmol/retina following 24h of dark adaptation, respectively (Figure 12C). The calculated regeneration rates following a strong bleach were 6.3 pmol/min in wild-type animals and 4.9 pmol/min in R91W/wt; indicating slightly slower rhodopsin regeneration kinetics in R91W/wt animals.

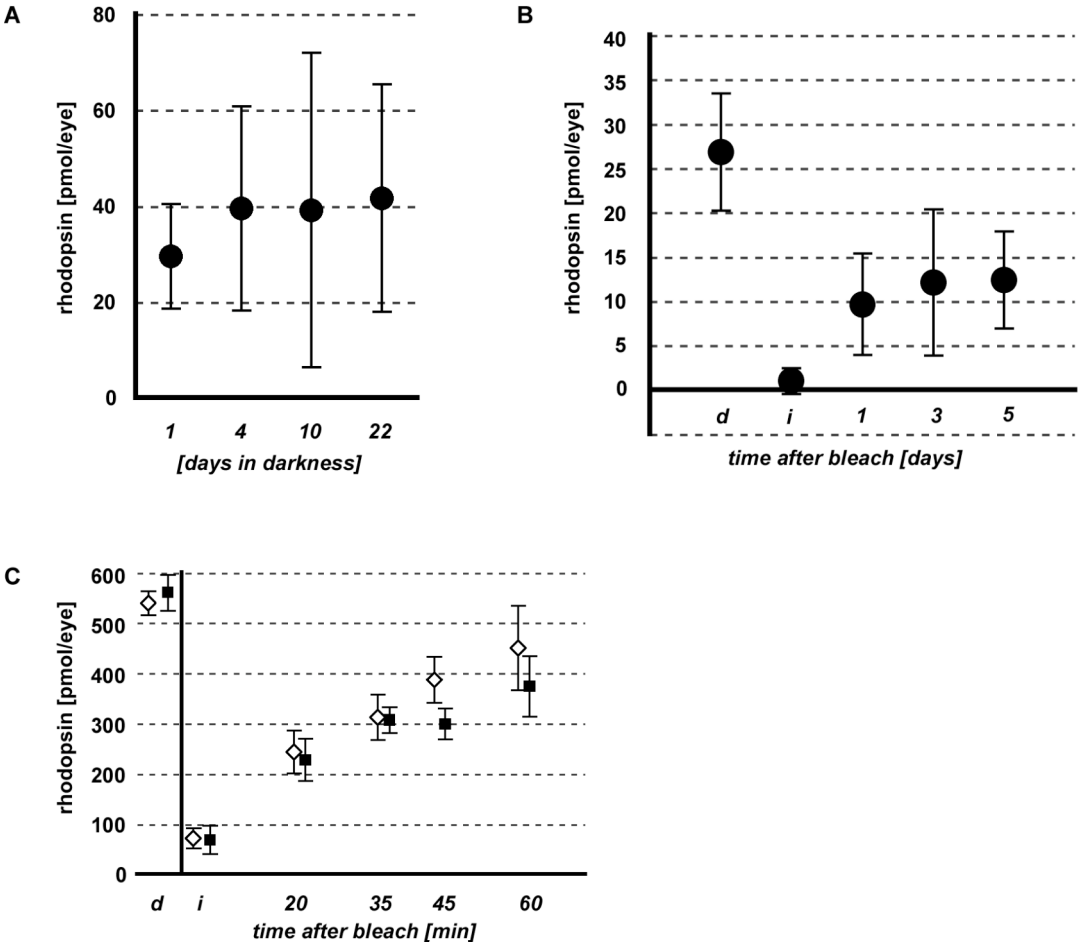

Figure 12 Rhodopsin content and regeneration kinetics

A, Rhodopsin levels in 6 to 7 week-old R91W animals kept in darkness for 1 day or up to 22 days (as indicated).

B, Rhodopsin regeneration of R91W mice. Following 24 h dark-adaptation, R91W mice were exposed to 5'000 lux for 10 min and the rhodopsin content was analyzed immediately (i) or after different periods of recovery in darkness (indicated in days). Unexposed, dark-adapted mice (d) served as controls.

C, Rhodopsin regeneration of wild-type and R91W/wt heterozygous mice. Following 24 h dark-adaptation, mice were exposed to 5'000 lux for 10 min and the rhodopsin content was analyzed immediately (i) or after different periods of recovery in darkness (indicated in minutes). Unexposed, dark-adapted mice (d) served as controls. Note the slightly slower regeneration kinetics in R91W/wt mice.
Filled squares, R91W/wt; open squares wild-type.

All values are given in pmol/eye ± S.D. At least three animals per condition and genotype were analyzed.

3.5 Photoreceptor function in R91W mutant mice

The previous experiments showed that R91W mice contain detectable amounts of the 11-*cis* chromophore suggesting that some visual function might be retained. This function was tested under scotopic conditions by single flash ERG with increasing light intensities ranging from 0.1 mcd*s/m^2 to 25 cd*s/m^2. ERG recordings revealed that higher intensities of light are needed to induce an electrical response in R91W as compared to wild-type mice (Figure 13A top panel). By assessing the luminance required to generate a half maximal b-wave, the reduction in light sensitivity (Machida et al. 2000) of 8 weeks-old R91W mice was determined to be approximately 2.6 log units, as compared to wild-type. In age series testing 8, 12, 24 and 40 week-old animals the sensitivity threshold remained unaltered, while the b-wave amplitude was reduced with increasing age in R91W, which was especially prominent between 12 and 24 weeks (Figure 13A bottom panel). From 24 weeks of age no further reduction in b-wave amplitude was detected. Qualitatively, the ERG response of the R91W mice showed no distinct a-wave under the conditions applied, suggesting compromised rod function (Figure 13A overlay).

In order to test cone function, ERG responses were recorded under photopic conditions by increasing flash intensities from 10 mcd*s/m^2 to 25 cd*s/m^2 (Figure 13B). Notably, there was no difference in threshold sensitivity or in amplitude of the b-wave in 8 week-old age matched R91W and wild-type control animals (Figure 13B top and bottom panel). The remarkable similarity of responses recorded under normally cone-isolating conditions between R91W and wild-type animals is illustrated by the overlay in Figure 13B taken at 25 cd*s/m^2 light intensity. However, differences in oscillatory potentials in the leading edge of the b-wave and a prominent delayed peak, suggested disparities, needing further investigation.

The threshold light (1 cd*s/m^2) exerted responses of similar amplitude at all ages. In contrast, and as observed under scotopic conditions, the amplitude of the b-wave at higher flash intensities was reduced with age up to 24 weeks (Figure 13B bottom panel). Thus, while the sensitivity of the retina was not prone to age-related reduction, the maximal response size was.

Comparison of wild-type and R91W/wt heterozygous animals resulted, as expected, in no difference between the genotypes under scotopic (Figure 13C) or photopic (Figure 13D) conditions.

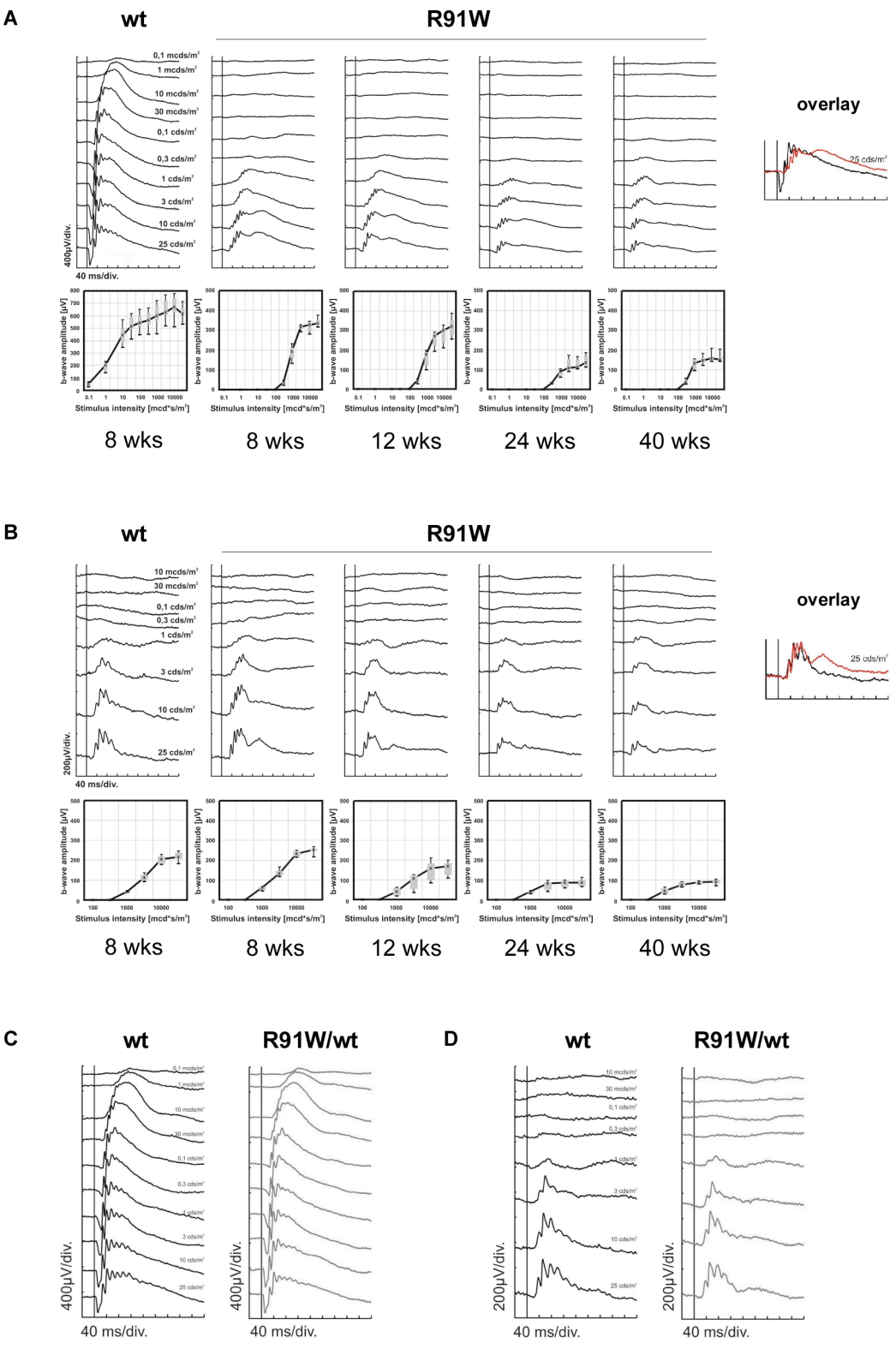

Figure 13 Assessment of photoreceptor function in R91W mutant mice

ERG response to single-flash stimuli with increasing flash intensities in 8, 12, 24 and 40 weeks-old R91W and compared to wild-type and R91W/wt heterozygous mice.

A, Scotopic single-flash ERG indicating loss of sensitivity (app. 2.6 log units) in R91W animals as compared to 8 week-old wild-type. The b-wave amplitudes were plotted against stimulus intensity at

indicated ages (lower panels). A steady decline in the b-wave amplitude was detected with increasing age. However, retinal sensitivity as determined by the lowest light intensity triggering a response remained largely unchanged. Overlay: Note the absence of a typical a-wave (initial downward deflection) in R91W mice (red trace).

B, Photopic single-flash ERG reflecting an equal sensitivity and similar shape of response between wild-type and R91W animals at 8 weeks of age. There was a steady decline of the b-wave amplitude with increasing age. Overlay: Note the similar shape of the initial responses, with a distinctive second peak in R91W mice (red trace).

C, Scotopic- and (D) photopic- single-flash ERG responses in R91W/wt are comparable to wild-type animals. Representative recordings are shown for age matched 12 week-old animals.

Luminance response function curves are representative traces from individual animals. Each statistical graph (lower panels in A and B) represents data obtained from 3 mice e.g. 6 eyes. Boxes indicate the 25% and 75% quantile range, whiskers indicate the 5% and 95% quantile and the asterisk indicates the median of the data.

3.6 Assessment of retinal morphology

The functional tests performed suggested an age-related degenerative process caused by the R91W mutation, as the b-wave amplitudes of both: scotopic and photopic responses were reduced with increasing age (Figure 13A and B).

The complete lack of Rpe65 expression leads to a slow retinal degeneration evidenced relatively early by less densely packed rod outer segments and at later stages by the loss of photoreceptor nuclei (Redmond et al. 1998; Woodruff et al. 2003). In human patients carrying mutations in RPE65, the assessment of retinal degeneration by optical coherence tomography (OCT) likewise revealed a thinned photoreceptor layer (Van Hooser et al. 2000; Lorenz et al. 2004; Jacobson et al. 2005).

To analyze retinal morphology in more detail, we compared four different genotypes (wild-type, R91W/wt, R91W and Rpe65$^{-/-}$) at various ages (from 4 weeks till 1 year) using light microscopy (Figure 14). Already at 4 weeks of age the outer segments (OS) of R91W and Rpe65$^{-/-}$ mice showed first signs of disorganization (Figure 14, top row). Pathological changes affecting photoreceptors such as reduced compactness and shortening of outer segments became more obvious as the mice grew older. Although the thickness of the outer nuclear layer (ONL) at earlier time-points was comparable to wild-type, only 5 rows of nuclei remained in the central area of 1 year-old mutant animals, as compared to 9-10 rows in one-year old wild-type.

In comparison to Rpe65$^{-/-}$ animals, R91W mice showed a slightly better preservation of OS, at least up to 12 weeks of age (Figure 14, compare last two columns). Of note, R91W mice seemed to contain more cone nuclei than respective age-matched Rpe65$^{-/-}$ mice especially at early ages, which was further analyzed in detail.

At all ages analyzed, we did not find differences between the retinal morphology of wild-type and R91W/wt heterozygous mice (Figure 14; compare first two columns), which is in line with a recessive inheritance of the phenotype caused by the R91W mutation. Furthermore, no morphologic differences between all tested genotypes were detected in the inner retinal structures upon examination by light microscopy.

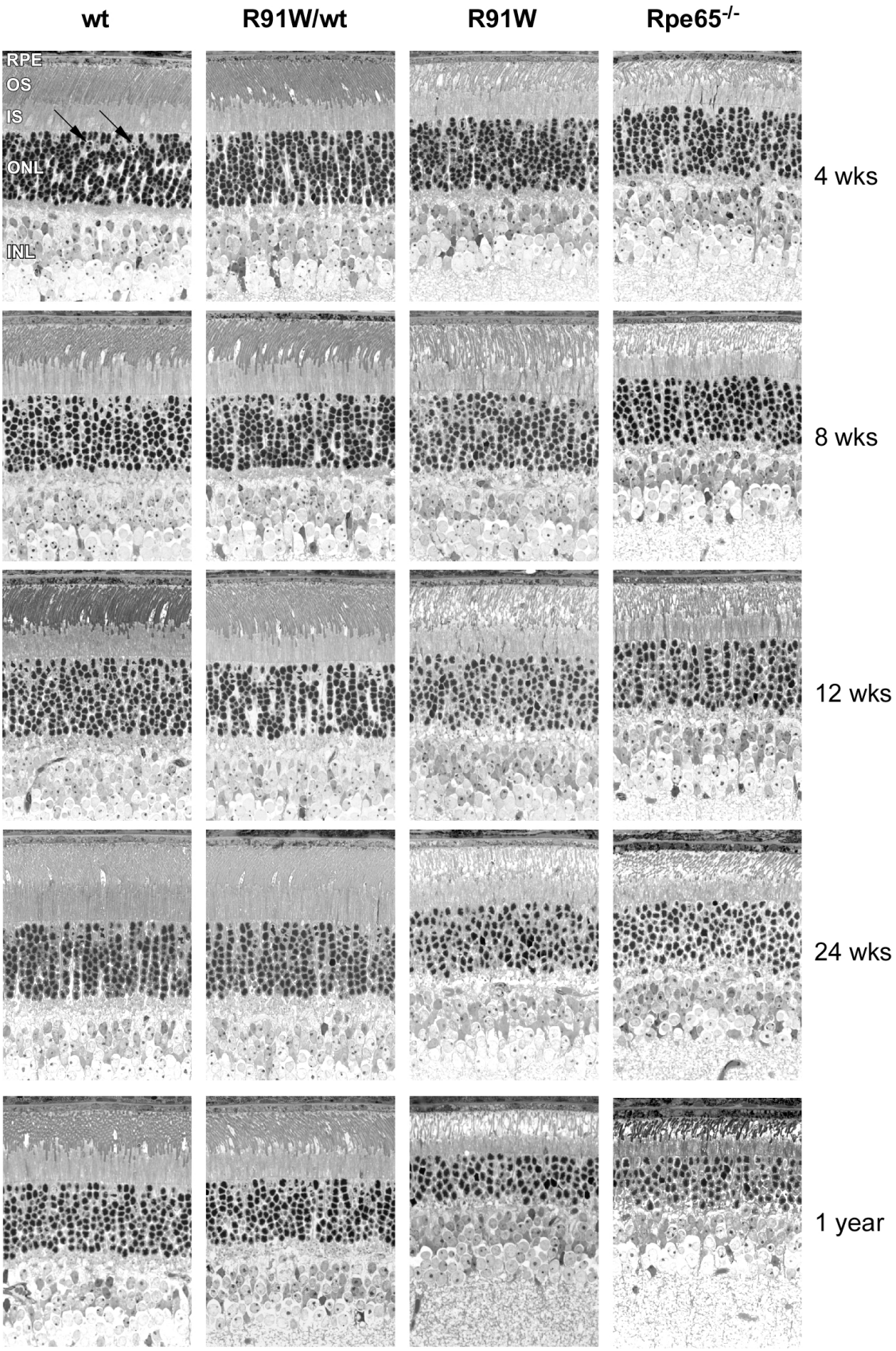

Figure 14 Light microscopic changes in R91W retinas in comparison to wild-type, R91W/wt and Rpe65$^{-/-}$ mice at various ages

Figure 14, continued

The thickness of the ONL in R91W mice remained nearly normal until 24 weeks, however, already at 8 weeks more voids were visible in this layer accompanied by the appearance of pycnotic nuclei. By 1 year, only 5 to 6 rows of nuclei remained in the ONL. Disorganization of OS was evident in R91W mice already at 4 weeks of age and became more pronounced with ageing. Between 24 weeks and 1 year of age OS were greatly shortened. As compared to $Rpe65^{-/-}$ mice, R91W mice showed better retinal preservation at least at earlier ages evidenced especially by longer OS and their higher density. Another distinctive feature was the relative better preservation of cone nuclei in younger R91W animals as compared to age-matched $Rpe65^{-/-}$ mice. At all time-points no difference was observed between wild-type and R91W/wt animals.

RPE, retinal pigment epithelium; INL, inner nuclear layer; IS, inner segments; ONL, outer nuclear layer; OPL, outer plexiform layer; OS, outer segments. Arrow in the ONL indicates cone nuclei characterized by less densely packed chromatin.

3.7 Cones are functional in R91W

11-*cis* retinal is the chromophore of both rods and cones. It has been shown that ablation of Rpe65 eliminates cone function and remnant minimal visual responses can be attributed to rod function due to the presence of 9-*cis* retinal forming isorhodopsin (Seeliger et al. 2001; Fan et al. 2003). R91W mice contain similar amounts of 9-*cis* retinal but, in contrast to Rpe65$^{-/-}$ mice, they also contain 11-*cis* retinal (Table 4; Figure 12A, B). The functional tests performed (Figure 13) suggested that the rod system in R91W is severely affected, while cone function might be preserved especially in younger animals. To test more selectively for the source of visual function in the mutant mice we abolished rod function in R91W mice by generating R91W;Rho$^{-/-}$ double mutant mice and compared them to single mutant (R91W or Rho$^{-/-}$) or double mutant (Rpe65$^{-/-}$;Rho$^{-/-}$) mice. Rho$^{-/-}$ mice lack the rod opsin apoprotein and therefore cannot generate a rod derived visual response (Jaissle et al. 2001). Their retina is functionally considered a cone-only retina.

A dark-adapted ERG intensity series of 4 week-old wild-type, single mutant (R91W, Rho$^{-/-}$) and double mutant (R91W;Rho$^{-/-}$ and Rpe65$^{-/-}$;Rho$^{-/-}$) mice was recorded. All of the mutant mice showed severely depressed ERG responses as compared to the wild-type (Figure 15A; compare II, III, IV, V to I; Figure 15B, C). In scotopic conditions we found that the retinas of R91W mice and Rho$^{-/-}$ have a comparable light sensitivity (Figure 15A; compare II to IV). The oscillatory potentials in the leading edge of b-wave and higher b-wave amplitude (Figure 15A; compare II to IV) detected probably reflect better inner retinal preservation in R91W mice as compared to Rho$^{-/-}$ mice. In R91W;Rho$^{-/-}$ mice only high intensity flashes induced minimal responses that were even further reduced in amplitude (Figure 15A; III). In Rpe65$^{-/-}$;Rho$^{-/-}$ mice double mutants, as reported by Seeliger et al., no response was detected upon stimulation with any intensity of light (Figure 15A; V)(Seeliger et al. 2001).

To study cone responses, photopic flash intensity series across a 6-log-unit intensity range have been recorded in 4 week-old mice of the 5 genotypes described above (Figure 16A, B and C). Under the rod-suppressing conditions, comparison between the wild-type, R91W and Rho$^{-/-}$ revealed very similar threshold sensitivity (Figure 16A; compare I, II, and IV). Additional ablation of rhodopsin in R91W (R91W;Rho$^{-/-}$) resulted in 1.5 log units shift in sensitivity (Figure 16A; compare III to I, II and IV). However, the most striking difference was obtained when R91W;Rho$^{-/-}$ mice

were directly compared to Rpe65$^{-/-}$;Rho$^{-/-}$ mice (Figure 16A; compare III to V), where the latter mice virtually have no response at all. Collectively, these data prove that cones are functional in R91W mice at least at early ages.

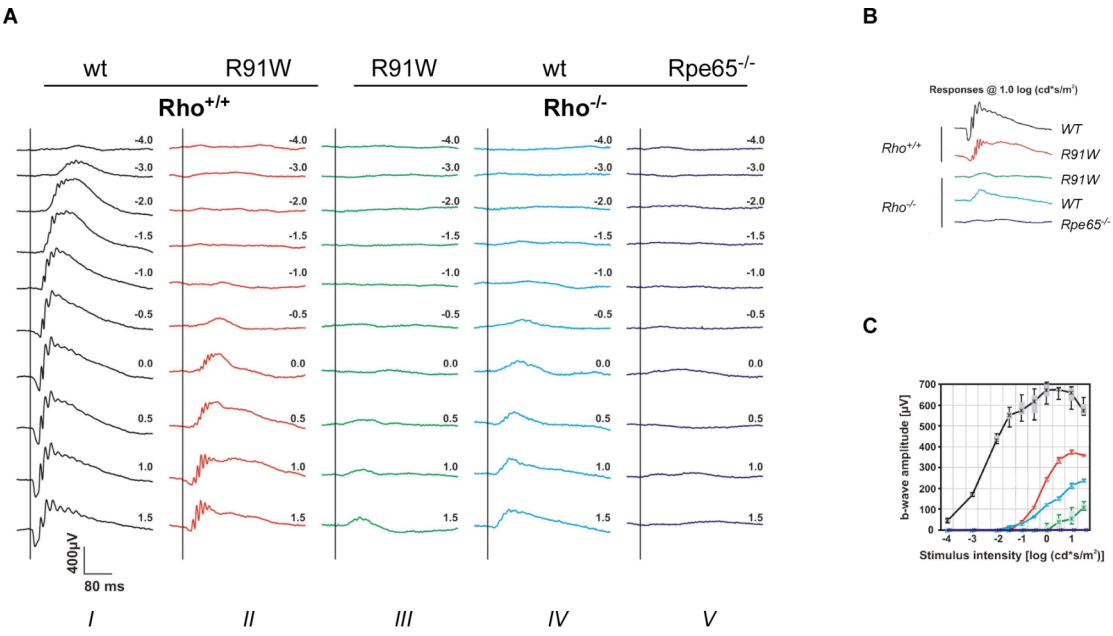

Figure 15 Scotopic ERGs in mice of different Rpe65 status

Scotopic ERG responses to single-flash stimuli with increasing flash intensities in 4 weeks-old animals of different Rpe65 status (wild-type, R91W knock-in or Rpe65 knock-out) in presence or absence of functional rhodopsin (Rho).

A, Loss of sensitivity in R91W animals as compared to 4 week-old wild-type having normal rhodopsin (compare I to II). Minimal or no responses were detected in mouse strains on a rhodopsin knock-out background (III, IV, V) at low light intensities. Responses at higher intensities demonstrate cone function. Only Rpe65$^{-/-}$;Rho$^{-/-}$ (V) animals had no recordable ERG response

B, Comparative representation of responses recorded in all tested genotypes at 1 log cd*s/m^2 light intensity.

C, The b-wave amplitudes plotted against stimulus intensity in all tested strains indicate reduced amplitude of response and sensitivity in all mutant mice. Note the complete lack of response in Rpe65$^{-/-}$; Rho$^{-/-}$ mice. Color coding for mouse strains as in A and B.

Luminance response function curves (in Fig. A) are representative traces from individual animals. Statistical graphs (in Fig. C) represent data obtained from wt;Rho$^{+/+}$, R91W;Rho$^{+/+}$, R91W;Rho$^{-/-}$(n=3, respectively), wt;Rho$^{-/-}$ (n=1) and Rpe65$^{-/-}$;Rho$^{-/-}$ (n=2). Boxes indicate the 25% and 75% quantile range, whiskers indicate the 5% and 95% quantile and the asterisk indicates the median of the data.

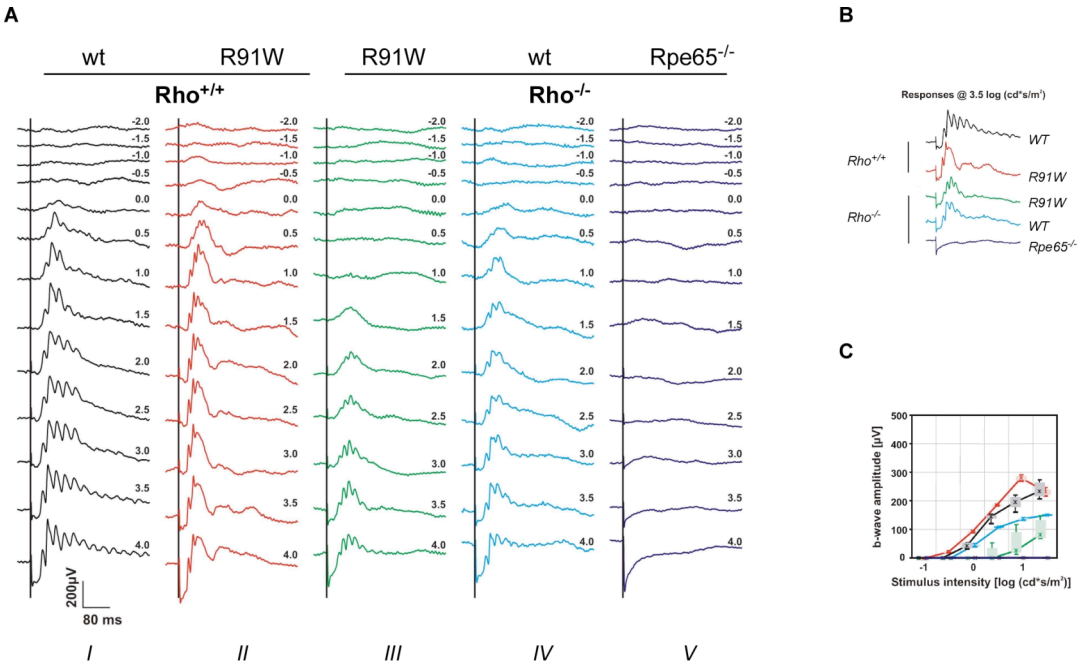

Figure 16 Cone function is preserved in R91W mice

Photopic ERG responses to single-flash stimuli with increasing flash intensities in 4 weeks-old animals of different Rpe65 status (wild-type, R91W knock-in or Rpe65 knock-out) in presence or absence of functional rhodopsin (Rho).

A, Photopic ERG reflecting an equal sensitivity and similar shape of response between wild-type and R91W animals having normal rhodopsin and wild-type Rpe65 on a rhodopsin knock-out background (compare I, II and IV). A shift in sensitivity was detected in R91W mice on a rhodopsin knock-out background as compared to the above mentioned animals (compare III to I, II, IV). No response was recorded in $Rpe65^{-/-}$;$Rho^{-/-}$ animals (V).

B, Comparative representation of responses recorded in all tested genotypes at 3.5 log cd*s/m^2 light intensity.

C, The b-wave amplitudes plotted against stimulus intensity in all tested strains indicating reduced sensitivity in R91W; $Rho^{-/-}$ animals. Note complete lack of response in $Rpe65^{-/-}$; $Rho^{-/-}$ mice. Color coding for mouse strains as in A and B.

Luminance response function curves (in Fig. A) are representative traces from individual animals. Statistical graphs (in Fig. C) represent data obtained from wt;$Rho^{+/+}$, R91W;$Rho^{+/+}$, R91W;$Rho^{-/-}$(n=3, respectively), wt;$Rho^{-/-}$ (n=1) and $Rpe65^{-/-}$;$Rho^{-/-}$ (n=2). Boxes indicate the 25% and 75% quantile range, whiskers indicate the 5% and 95% quantile and the asterisk indicates the median of the data.

3.8 Reduction in cone and rod markers

Previous studies in Rpe65$^{-/-}$ mice have shown that cone markers are reduced very early in postnatal development and that RPE65 gene delivery or 9- or 11-*cis* retinal administration prevents the downregulation of cone-specific genes (Znoiko et al. 2005; Chen et al. 2006b). The authors of the above studies hypothesized that chromophore starvation may be responsible for the early cone degeneration.

We examined the mRNA levels in 4, 8, 12 and 24 week-old R91W and corresponding wild-type animals for both cone- and rod-specific markers (Figure 17A and B). Red cone opsin (middle wave length; MWL) expression was reduced to 65% already at 4 weeks of age (Figure 17A) and by 24 weeks only 47% of wild-type levels were expressed. The blue cone opsin (short wave length; SWL) was even more suppressed: 23% in 4 weeks and 8% in 24 week-old animals (Figure 17A). Expression of cone-specific transducin alpha-subunit (Gnat2) was reduced between 43-26% (Figure 17A).

A reduction of rod-specific markers has not been observed in Rpe65$^{-/-}$ animals up to 8 weeks of age (Znoiko et al. 2005). In R91W animals rod opsin mRNA levels were reduced down to 41% of wild-type levels already at 4 weeks of age and remained reduced up to 24 weeks (Figure 17B). A similar reduction of expression was detected for the rod-specific transducin alpha-subunit (Gnat1) (Figure 17B).

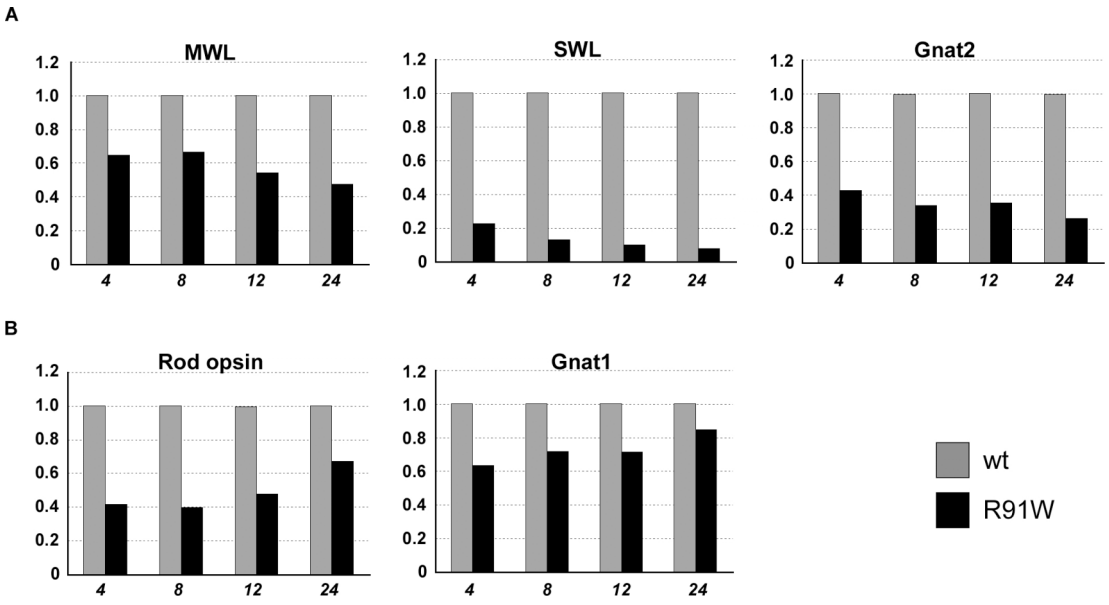

Figure 17 Reduction in cone and rod RNA markers

Relative levels of the indicated cone markers (A), and rod markers (B). The expression of markers was quantified in retinas of wild-type and R91W mice at 4, 8, 12 and 24 weeks of age by real-time RT-PCR. mRNA levels are expressed relative to the level of age matched wild-type control, which was set to 1. RNA isolated from 2 independent retinas per time-point and genotype was amplified in triplicates.

MWL, middle wave length cone opsin; Gnat1, rod-specific transducin alpha-subunit; Gnat2, cone-specific transducin alpha-subunit; SWL, short wave length cone opsin.

We additionally analyzed the cone markers by immunostaining in 4, 8, 16, 32 and 40 weeks and quantified the number of cells positive for GNAT2, MWL and SWL-cone opsin (Figure 18). As compared to wild-type controls, the 4 week-old R91W animals showed reduction in all three tested cone markers. The total Gnat2, MWL and SWL positive cells were reduced by 35, 62 and 59%, respectively (data not shown).

Znoiko at all showed that Rpe65$^{-/-}$ mice exhibited significant cone loss in the ventral retina at very early ages (Znoiko et al. 2005). A dorso-ventral gradient of expression for MWL and SWL cones has been described in the mouse retina (Applebury et al. 2000). In order to analyze the spatial distribution of cones and the suspected age-dependent cone loss we quantified the dorso-ventral cone distribution in 8, 16, 42, 32 and 40 week-old R91W and compared it to 4 week-old R91W animals set as 100% for dorsal, ventral or total expression (Figure 18). The analyzed retinal area is described in the methods. By 8 weeks of age the most prominent cone loss occurred in the ventral retina where GNAT2 and MWL opsin were reduced by 80% and SWL opsin by 70% as compared to their levels in 4 week-old animals (Figure 18). By 16 weeks of age the ventral retina was cone-free. In the dorsal retina between 4 and 8 weeks GNAT2 remained stable, but was reduced to 40% by 24 weeks of age. After 32 weeks of age, GNAT2 positive cells were no longer detectable (Figure 18). A very similar pattern in reduction of SWL and MWL opsin containing cones has been detected during the ageing in dorsal retina (Figure 18) but to a lesser extent.

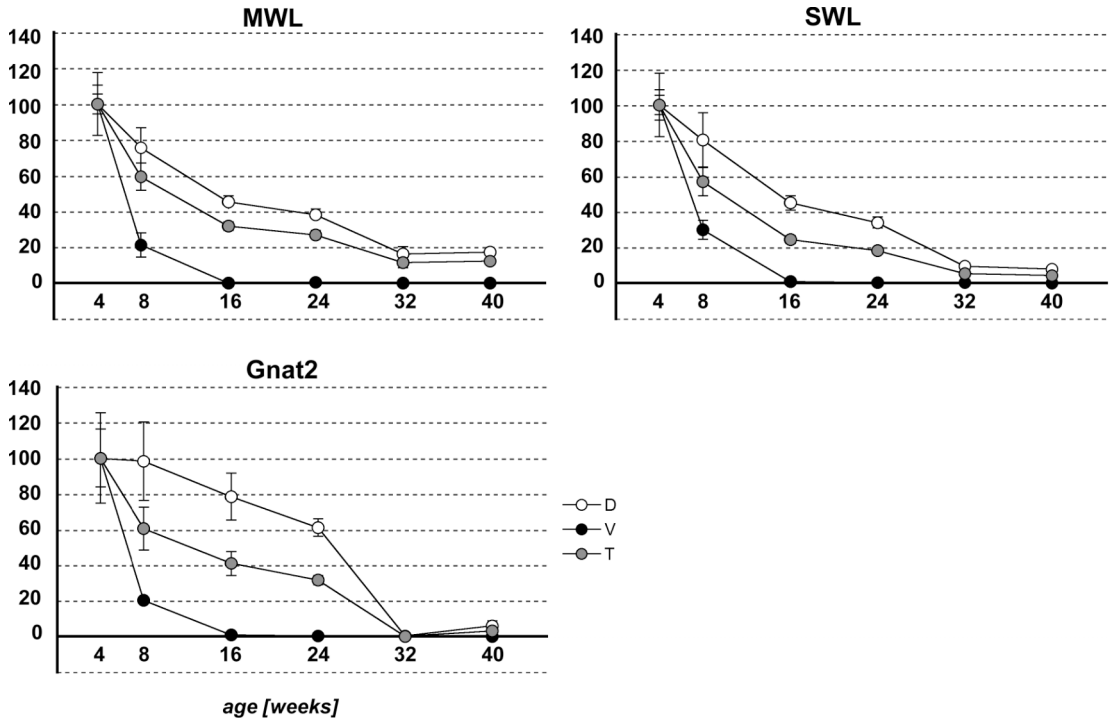

Figure 18 Geographical distribution and temporal cone cell loss caused by R91W mutation

Cones were quantified by counting the number of MWL-, SWL- or GNAT2- positive outer segments in dorso-ventrally oriented retinal sections cut trough the optic nerve.

Graphs represent percentages of 4 week-old R91W (set to 100%) for a given cone-marker and region of retina (mean ± S.D.). An age-dependent decrease of cone marker labeling was observed that led to an almost complete disappearance of cones at 32 weeks of age.

D, dorsal; V, ventral; T, total (represents sum of dorsal and ventral positive signals)

3.9 Degeneration markers

The morphological analysis at 4 weeks of age showed that the OS of R91W were slightly disorganized (Figure 14). At this time-point expression of glial fibrillary acidic protein (GFAP) mRNA, a marker of retinal gliosis, was upregulated 3 fold (Figure 19). Similar GFAP expression-levels were detected at 8 weeks but increased later to a maximal 10-fold induction in 24 week-old mutant mice (Figure 19). Caspase-1, another marker for retinal degeneration in induced (Grimm et al. 2000) and inherited models (Samardzija et al. 2006), was expressed at relative low levels in younger animals (Figure 19). However, at 12 and 24 weeks of age, a 3- and 5.5-fold induction was detected, respectively. Increased expression of the stress-inducible protein fibroblast growth factor 2 (FGF2) has been detected in inherited and induced models for retinal degeneration (Gao and Hollyfield 1996; Samardzija et al. 2006). In R91W mice, upregulation of FGF2 was detected as early as 4 weeks after birth; and 24 week-old animals expressed 10-fold higher FGF2 levels than age-matched wild-types (Figure 19).

Comparable low expression of degeneration markers was detected at all time-points in wild-type and R91W/wt animals (not shown), indicating that one mutant allele of Rpe65 is insufficient to trigger pathological changes on retinal morphology.

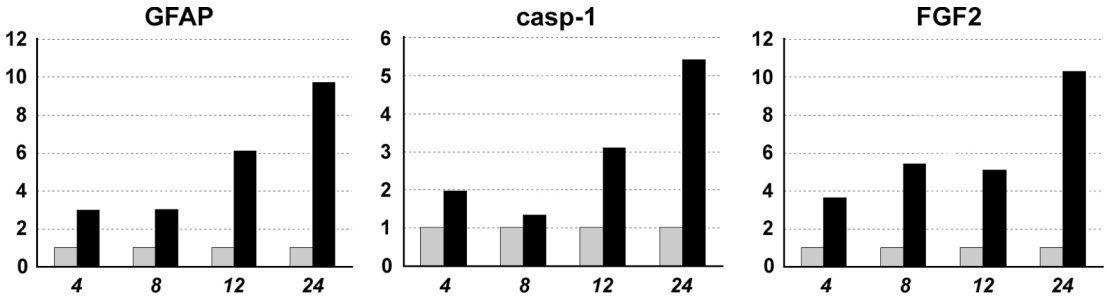

Figure 19 Retinal degeneration markers are induced in R91W

Relative mRNA levels of GFAP, Casp-1 and FGF2 in retinas of wild-type and R91W at 4, 8, 12 and 24 weeks of age as determined by real-time RT-PCR. mRNA levels are expressed relative to age-matched wild-type controls, which were set to 1. RNA isolated from 2 independent retinas per time-point and genotype was amplified in triplicates (means ± S.D.).

4 DISCUSSION

4.1 R91W knock-in mice: close correlation with the human phenotype

R91W mice represent the first knock-in animal model of a human blinding disease that exactly reproduces the mutation identified in patients. The analyses in the present work clearly show that for understanding a particular disease, reproducing a mutation is superior to a “simple” knock-out of the gene in question.

To date, more than 80 mutations have been identified in the Rpe65 gene of patients with inherited retinal dystrophies (summarized in (Zernant et al. 2005)). More than 60% of them are missense mutations. It has been shown that different mutations in Rpe65 are associated with variability in the severity of retinal dystrophy (Hamel et al. 1999; Lorenz et al. 2000). This may be explained by the different functional consequences of the various mutations. However, up to now, all available animal models ($Rpe65^{-/-}$ mice; naturally occurring rd12 mice and Swedish Briard dogs) are carrying a functionally null allele of the Rpe65 gene.

Our comparative studies of different mice with selective impairment of rod function demonstrated that cones are functional in R91W knock-in mice. This is in accordance with the phenotypical characterization of R91W patients that are diagnosed with EOSRD. These patients typically have congenital night-blindness but retain cone-mediated vision in childhood sufficient to acquire reading in the first decade (El Matri et al. 2006). In addition, other reports on patients carrying a mutation in Rpe65 demonstrate functional central, that is cone vision early in life (summarized in (Paunescu et al. 2005)). As opposed to this relatively mild phenotype, another phenotype of the Rpe65-diseases is characterized as legally blind at birth or severely visually impaired in infancy. These patients are diagnosed as LCA.

The observations from R91W patients were not in line with data from Rpe65 deficient mice. $Rpe65^{-/-}$ mice clearly have no cone function and residual visual function in these mice is attributed to desensitized rods supplied with endogenous 9-*cis* retinal as a chromophore (Seeliger et al. 2001; Fan et al. 2003).

The work presented here suggests, as hypothesized before, that the level of RPE65 impairment (e.g. functional null vs. mutant protein) might control the rate at which photoreceptors degenerate (Hamel et al. 1999).

4.2 R91W knock-in mice: metabolic changes induced by the mutation

Only recently the enzymatic role of RPE65 as the isomerohydrolase in the visual cycle was revealed by several studies in heterologous expression systems (Jin et al. 2005; Moiseyev et al. 2005; Redmond et al. 2005; Takahashi et al. 2005). In these studies a minimal visual cycle has been restored in cell lines different from RPE and only cells transfected with RPE65 vectors produced 11-*cis* retinoids. In parallel, studies using the same experimental paradigm were undertaken aiming at understanding the pathological changes caused by mutations in Rpe65 shown to be associated with human disease (Redmond et al. 2005; Chen et al. 2006a; Takahashi et al. 2006). In particular, a study on $Rpe65^{R91W}$ showed that this mutation causes decreased RPE65 protein levels due to a decreased protein stability and/or protein mislocalisation (Takahashi et al. 2006). However, in the same report no isomerohydrolase activity of mutant $Rpe65^{R91W}$ protein was detectable.

To circumvent the limitations of the *in vitro* heterologous expression systems, Chen et al. employed a different strategy: They delivered mutant Rpe65 to the RPE of Rpe65 deficient mice by means of an adenoviral vector (Chen et al. 2006b). Using this approach, these authors were aiming at RPE65 expression in a more “natural” context. Interestingly, this strategy produced results similar to those obtained *in vitro*. In particular, the expression of $Rpe65^{R91W}$ from a viral vector did not result in detectable immunostaining of the mutant protein in the RPE and accordingly did not result in a gain of retinal function.

In contrast to R91W expressed in the above-mentioned *in vitro* or *in situ* systems, R91W expressed as a knock-in gene resulted in: 1) detectable protein expression with a correct localization to the RPE and 2) metabolic activity evidenced by generation of 11-*cis* retinal.

R91W knock-in mice as introduced in this work are the most natural system to analyze effects of the mutation. The cellular context, temporal expression and genetic regulation are as close as possible to the natural situation – with striking consequences on the results of the analysis. These data demonstrate that a true assessment of the

characteristics of a mutant gene / protein may only be possible, by using the knock-in technology.

4.3 R91W knock-in mice: changes in the visual cycle

RPE65 is a protein preferentially and abundantly expressed in the RPE microsomal fraction (Hamel et al. 1993a; Seeliger et al. 2001; Hemati et al. 2005). The catalytic role of RPE65 as isomerohydrolase in the visual cycle has been established recently: In conjunction with LRAT, RPE65 is necessary to synthesize 11-*cis* retinol from all-*trans* retinyl esters (Jin et al. 2005; Moiseyev et al. 2005; Redmond et al. 2005). Thus, it catalyzes a key-reaction of the visual cycle, essential to form 11-*cis* isomers out of all-*trans* isomers. Apparently, RPE65 is the only protein of the RPE able to catalyze this reaction as in its absence 11-*cis* isomers cannot be formed (Redmond et al. 1998).

Like the wild-type protein, the mutant $RPE65^{R91W}$ was expressed exclusively in the RPE, but at dramatically reduced levels (5% of wild-type levels). As the RNA levels of Rpe65 in wild-type and in R91W knock-in mice were comparable, the reason for the reduced amount of mutant RPE65 protein might be at the translational or post-translational stage. Recently, in agreement with our quantitative data, an *in vitro* study showed that the R91W mutation causes decreased RPE65 protein levels due to a decreased protein stability and/or protein mislocalisation of the protein with subsequent degradation (Takahashi et al. 2006).

Comparing Rpe65 knock-out with Rpe65 R91W knock-in mice revealed several differences with regard to the visual cycle, the most important one being the limited, but measurable ability of R91W knock-in mice to generate 11-*cis* retinal. The measurable amounts of 11-*cis* retinal indicate that the visual cycle in R91W mutant mice is operative, even though at a strongly reduced rate. Rhodopsin amounts are linearly correlated with amounts of 11-*cis* retinal (Wenzel et al. 2005). However, our quantitative assessment of rhodopsin showed that the maximal levels of rhodopsin in R91W knock-in mice were 40 pmol, which is <10% of wild-type, and did not reach the wild-type amounts even after extended rearing for several days in darkness. Thus, although the apo-protein opsin is present at levels exceeding 10% of wild-type, only a small fraction was equipped with chromophore. The nature of this limitation is currently under investigation.

Another unexpected limitation of the visual cycle was revealed in experiments using a short exposure to bright light to bleach rhodopsin. Normal mice can recover their rhodopsin from such a bleach within 1-3 hours (Wenzel et al. 2001). R91W mice did not recover rhodopsin to dark-adapted levels within days. This may suggest that in addition to the limitation mentioned above, a strong bleach has an additional adverse effect on retinal physiology in a way which prevents 11-*cis* retinal from binding to opsin and/or which inhibits the formation of 11-*cis* retinal. Again, the underlying hindrance of the visual cycle remains to be investigated.

Despite this remnant RPE65 function, the all-*trans* retinyl ester substrate of the isomerohydrolase reaction accumulates in the R91W knock-in mouse comparable to RPE65 knock-out mice. Based on the quantification of rhodopsin, the majority of rod opsin in R91W mice was in an unliganded state. As 11-*cis* retinal acts as an inverse agonist, its absence will cause an increased spontaneous activity of the opsin molecule, leading to a constitutive activation of the phototransduction cascade (Bond et al. 1995; Kefalov et al. 1999). It has been hypothesized that due to the presence of unliganded opsin retina sends a signal that causes mobilization of retinol from blood circulation and its retention in RPE in retinyl ester form (Van Hooser et al. 2002). Thus, an insufficient supply with 11-*cis* retinal, particularly after bleaching, in R91W mice may cause the accumulation of similar amounts of retinyl esters as in $Rpe65^{-/-}$ mice.

Another highly hypothetical possibility is that 11-*cis* retinal detected in R91W mice originates not from the rod but from the proposed cone visual cycle (Mata et al. 2002). In this alternate pathway the cone pigment is regenerated independently of RPE and it is proposed to take place in Müller cells. However, enzymes for proposed catalytic steps of the cone pigment regeneration are still not cloned. Hypothetically, a cone visual cycle could be less affected by the R91W mutation; or even be fully operational. This was evidenced by the light-adapted (cone-specific) ERG having equal sensitivity and very similar shape of the response. How would the rods acquire 11-*cis* retinal in this case? 11-*cis* is covalently bound to rod opsin via a protonated Shiff base and this binding is irreversible. The cone opsin /11-*cis* retinal complex is less stable and it has been shown recently in amphibian red cones that the rate of 11-*cis* retinal spontaneous dissociation is approximately 10% (Kefalov et al. 2005). Given that even after the prolonged dark adaptation only 40 pmol of rhodopsin is produced or approximately 6% of wild-type rhodopsin, hypothetically this 11-*cis* retinal might be “stolen” by rods from neighboring cones due to spontaneous dissociation of chromophore. This might explain why rhodopsin regeneration kinetics is inefficient. However, this hypothesis is highly unlikely. Even though RPE65 has been detected in

cones (Ma et al. 1998; Znoiko et al. 2002) and disputed (Seeliger et al. 2001; Hemati et al. 2005) there is no experimental evidence that RPE65 is involved in the cone visual cycle. In addition, almost equal amounts of 11-*cis* retinal were retained up to 40 weeks of age, the time when the cones in R91W animals are almost completely lost.

4.4 Cone loss and degeneration

Cone loss was indicated by morphological data, functional studies, RNA expression and quantitative analysis of immunohistochemistry. The most affected retinal area was the ventral retina that was devoid of cones already at 16 weeks of age. It has been shown that the mouse ventral retina is enriched with SWL opsin (Applebury et al. 2000) and SWL cones are reduced particularly early in Rpe65$^{-/-}$ mice (Znoiko et al. 2005). Thus, qualitatively the geographic cone atrophy was similar between Rpe65 knock-out and R91W knock-in mice and in both the SWL cones were the most severely affected. However, in the knock-out, SWL cone opsin loss is more pronounced: SWL RNA is reduced by more than 95% by 4 weeks of age as opposed to less than 80% in R91W knock-in mice. For both models, it is not clear why SWL cones are especially prone to degeneration.

Not only do SWL cones appear to be better preserved in the R91W mouse, rather all cone-specific markers tested indicate that the cone system in R91W animals is less severely affected than in Rpe65 knock-out mice. Recently, Rohrer et al. detected cone opsin mislocalization in Rpe65$^{-/-}$ mice (Rohrer et al. 2005), which was corrected upon treatment of the mice with 11-*cis* retinal. Based on this observation, the authors hypothesized that cones degenerate because of opsin mislocalization as a direct result of 11-*cis* retinal starvation. This hypothesis might as well explain why cones in R91W mice are viable for extended periods of time.

Similarly, chromophore starvation has been indirectly implicated in rod degeneration in Rpe65$^{-/-}$ mice (Redmond et al. 1998; Seeliger et al. 2001), which exhibit a slow light-independent degeneration. Rod degeneration can be prevented by blocking rod specific G-protein transducin signaling (Gnat1) (Woodruff et al. 2003). Rpe65$^{-/-}$;Gnat1$^{-/-}$ double mutant animals accumulate similar amounts of retinyl esters as Rpe65$^{-/-}$ single mutants but nevertheless their rods are protected. Collectively these findings indicate that the probable cause of the degeneration in Rpe65$^{-/-}$ animals is permanent activation of the transduction cascade by unliganded opsin, and not the accumulation of retinyl esters (Woodruff et al. 2003). This concept is reinforced by the

observation that systemic supplementation with 11-*cis* retinal preserves photoreceptor structure despite continuing accumulation of retinyl esters. Accordingly, a better preservation and slower degeneration of retinal morphology in R91W in comparison to $Rpe65^{-/-}$ animals is probably attributable to the presence of 11-*cis* retinal. However, as the levels of 11-*cis* retinal were not exceeding 10% of wild-type levels during ageing, a large fraction of opsin may still have been in the unliganded e.g. activated state. Thus, also in R91W mice, the phototransduction cascade may be permanently activated, causing retinal degeneration. This possibility will be further investigated by breeding R91W mice with transducin knock-out animals, which is currently underway.

In summary, we generated a new mouse model for retinal dystrophy caused by a missense mutation in RPE65. More than 60% of the mutations identified in patients are missense mutations. There are striking differences to the knock-out situation, which are of importance for the understanding of the pathology and for clinical diagnosis. Furthermore, the therapeutic window for gene therapy – the first of which will be carried out these days in RPE65 patients – based on the results presented here may differ between patients with null- and missense mutations.

Preclinical trials for gene replacement are underway for the R91W knock-in mouse. A thorough analysis of the molecular pathways leading to SWL cone death and to rod degeneration will be conducted.

5 REFERENCES

Aguirre, G.D., Baldwin, V., Pearce-Kelling, S., Narfstrom, K., Ray, K., and Acland, G.M. 1998. Congenital stationary night blindness in the dog: common mutation in the RPE65 gene indicates founder effect. *Mol Vis* **4**: 23.

Applebury, M.L., Antoch, M.P., Baxter, L.C., Chun, L.L., Falk, J.D., Farhangfar, F., Kage, K., Krzystolik, M.G., Lyass, L.A., and Robbins, J.T. 2000. The murine cone photoreceptor: a single cone type expresses both S and M opsins with retinal spatial patterning. *Neuron* **27**(3): 513-523.

Arshavsky, V.Y., Lamb, T.D., and Pugh, E.N., Jr. 2002. G proteins and phototransduction. *Annu Rev Physiol* **64**: 153-187.

Batten, M.L., Imanishi, Y., Maeda, T., Tu, D.C., Moise, A.R., Bronson, D., Possin, D., Van Gelder, R.N., Baehr, W., and Palczewski, K. 2004. Lecithin-retinol acyltransferase is essential for accumulation of all-trans-retinyl esters in the eye and in the liver. *J Biol Chem* **279**(11): 10422-10432.

Baylor, D.A., Lamb, T.D., and Yau, K.W. 1979. Responses of retinal rods to single photons. *J Physiol* **288**: 613-634.

Bond, R.A., Leff, P., Johnson, T.D., Milano, C.A., Rockman, H.A., McMinn, T.R., Apparsundaram, S., Hyek, M.F., Kenakin, T.P., Allen, L.F., and et al. 1995. Physiological effects of inverse agonists in transgenic mice with myocardial overexpression of the beta 2-adrenoceptor. *Nature* **374**(6519): 272-276.

Boulanger, A., Liu, S., Yu, S., and Redmond, T.M. 2001. Sequence and structure of the mouse gene for RPE65. *Mol Vis* **7**: 283-287.

Burns, M.E. and Baylor, D.A. 2001. Activation, deactivation, and adaptation in vertebrate photoreceptor cells. *Annu Rev Neurosci* **24**: 779-805.

Chen, P., Hao, W., Rife, L., Wang, X.P., Shen, D., Chen, J., Ogden, T., Van Boemel, G.B., Wu, L., Yang, M., and Fong, H.K. 2001. A photic visual cycle of rhodopsin regeneration is dependent on Rgr. *Nat Genet* **28**(3): 256-260.

Chen, Y., Moiseyev, G., Takahashi, Y., and Ma, J.X. 2006a. Impacts of two point mutations of RPE65 from Leber's congenital amaurosis on the stability, subcellular localization and isomerohydrolase activity of RPE65. *FEBS Lett* **580**(17): 4200-4204.

Chen, Y., Moiseyev, G., Takahashi, Y., and Ma, J.X. 2006b. RPE65 gene delivery restores isomerohydrolase activity and prevents early cone loss in Rpe65-/- mice. *Invest Ophthalmol Vis Sci* **47**(3): 1177-1184.

Dartnall, H.J., Bowmaker, J.K., and Mollon, J.D. 1983. Human visual pigments: microspectrophotometric results from the eyes of seven persons. *Proc R Soc Lond B Biol Sci* **220**(1218): 115-130.

Deng, C., Zhang, P., Harper, J.W., Elledge, S.J., and Leder, P. 1995. Mice lacking p21CIP1/WAF1 undergo normal development, but are defective in G1 checkpoint control. *Cell* **82**(4): 675-684.

Driessen, C.A., Winkens, H.J., Hoffmann, K., Kuhlmann, L.D., Janssen, B.P., Van Vugt, A.H., Van Hooser, J.P., Wieringa, B.E., Deutman, A.F., Palczewski, K., Ruether, K., and Janssen, J.J. 2000. Disruption of the 11-cis-retinol dehydrogenase gene leads to accumulation of cis-retinols and cis-retinyl esters. *Mol Cell Biol* **20**(12): 4275-4287.

Dryja, T.P., McGee, T.L., Reichel, E., Hahn, L.B., Cowley, G.S., Yandell, D.W., Sandberg, M.A., and Berson, E.L. 1990. A point mutation of the rhodopsin gene in one form of retinitis pigmentosa. *Nature* **343**(6256): 364-366.

El Matri, L., Ambresin, A., Schorderet, D.F., Kawasaki, A., Seeliger, M.W., Wenzel, A., Arsenijevic, Y., Borruat, F.X., and Munier, F.L. 2006. Phenotype of three

consanguineous Tunisian families with early-onset retinal degeneration caused by an R91W homozygous mutation in the RPE65 gene. *Graefes Arch Clin Exp Ophthalmol*.

Fan, J., Rohrer, B., Moiseyev, G., Ma, J.X., and Crouch, R.K. 2003. Isorhodopsin rather than rhodopsin mediates rod function in RPE65 knock-out mice. *Proc Natl Acad Sci U S A* **100**(23): 13662-13667.

Forrester, J.V., Dick, A.D., McMenamin, P.G., and Lee, W.R. 1996. The eye: basic sciences in practice. *WB Saunders company*.

Gao, H. and Hollyfield, J.G. 1996. Basic fibroblast growth factor: increased gene expression in inherited and light-induced photoreceptor degeneration. *Exp Eye Res* **62**(2): 181-189.

Ghyselinck, N.B., Bavik, C., Sapin, V., Mark, M., Bonnier, D., Hindelang, C., Dierich, A., Nilsson, C.B., Hakansson, H., Sauvant, P., Azais-Braesco, V., Frasson, M., Picaud, S., and Chambon, P. 1999. Cellular retinol-binding protein I is essential for vitamin A homeostasis. *Embo J* **18**(18): 4903-4914.

Grimm, C., Wenzel, A., Hafezi, F., and Reme, C.E. 2000. Gene expression in the mouse retina: the effect of damaging light. *Mol Vis* **6**: 252-260.

Hamel, C., Marlhens, F., Griffoin, J., Bareil, C., Claustres, M., and Arnaud, B. 1999. Different mutations in RPE65 are associated with variability in the severity of retinal dystrophy *Hollyfield, JG Anderson, RE LaVail, MM eds Retinal Degenerative Diseases and Experimental Therapy ,27 Kluwer Academic/Plenum New York*.

Hamel, C.P., Tsilou, E., Harris, E., Pfeffer, B.A., Hooks, J.J., Detrick, B., and Redmond, T.M. 1993a. A developmentally regulated microsomal protein specific for the pigment epithelium of the vertebrate retina. *J Neurosci Res* **34**(4): 414-425.

Hamel, C.P., Tsilou, E., Pfeffer, B.A., Hooks, J.J., Detrick, B., and Redmond, T.M. 1993b. Molecular cloning and expression of RPE65, a novel retinal pigment epithelium-specific microsomal protein that is post-transcriptionally regulated in vitro. *J Biol Chem* **268**(21): 15751-15757.

Hemati, N., Feathers, K.L., Chrispell, J.D., Reed, D.M., Carlson, T.J., and Thompson, D.A. 2005. RPE65 surface epitopes, protein interactions, and expression in rod- and cone-dominant species. *Mol Vis* **11**: 1151-1165.

Humphries, M.M., Rancourt, D., Farrar, G.J., Kenna, P., Hazel, M., Bush, R.A., Sieving, P.A., Sheils, D.M., McNally, N., Creighton, P., Erven, A., Boros, A., Gulya, K., Capecchi, M.R., and Humphries, P. 1997. Retinopathy induced in mice by targeted disruption of the rhodopsin gene. *Nat Genet* **15**(2): 216-219.

Jacobson, S.G., Aleman, T.S., Cideciyan, A.V., Sumaroka, A., Schwartz, S.B., Windsor, E.A., Traboulsi, E.I., Heon, E., Pittler, S.J., Milam, A.H., Maguire, A.M., Palczewski, K., Stone, E.M., and Bennett, J. 2005. Identifying photoreceptors in blind eyes caused by RPE65 mutations: Prerequisite for human gene therapy success. *Proc Natl Acad Sci U S A* **102**(17): 6177-6182.

Jaissle, G.B., May, C.A., Reinhard, J., Kohler, K., Fauser, S., Lutjen-Drecoll, E., Zrenner, E., and Seeliger, M.W. 2001. Evaluation of the rhodopsin knockout mouse as a model of pure cone function. *Invest Ophthalmol Vis Sci* **42**(2): 506-513.

Jin, M., Li, S., Moghrabi, W.N., Sun, H., and Travis, G.H. 2005. Rpe65 is the retinoid isomerase in bovine retinal pigment epithelium. *Cell* **122**(3): 449-459.

Katschinski, D.M., Marti, H.H., Wagner, K.F., Shibata, J., Eckhardt, K., Martin, F., Depping, R., Paasch, U., Gassmann, M., Ledermann, B., Desbaillets, I., and Wenger, R.H. 2003. Targeted disruption of the mouse PAS domain serine/threonine kinase PASKIN. *Mol Cell Biol* **23**(19): 6780-6789.

Kefalov, V.J., Carter Cornwall, M., and Crouch, R.K. 1999. Occupancy of the chromophore binding site of opsin activates visual transduction in rod photoreceptors. *J Gen Physiol* **113**(3): 491-503.

Kefalov, V.J., Estevez, M.E., Kono, M., Goletz, P.W., Crouch, R.K., Cornwall, M.C., and Yau, K.W. 2005. Breaking the covalent bond--a pigment property that contributes to desensitization in cones. *Neuron* **46**(6): 879-890.

Kloer, D.P., Ruch, S., Al-Babili, S., Beyer, P., and Schulz, G.E. 2005. The structure of a retinal-forming carotenoid oxygenase. *Science* **308**(5719): 267-269.

Kramer, R.H. and Molokanova, E. 2001. Modulation of cyclic-nucleotide-gated channels and regulation of vertebrate phototransduction. *J Exp Biol* **204**(Pt 17): 2921-2931.

Liou, G.I., Fei, Y., Peachey, N.S., Matragoon, S., Wei, S., Blaner, W.S., Wang, Y., Liu, C., Gottesman, M.E., and Ripps, H. 1998. Early onset photoreceptor abnormalities induced by targeted disruption of the interphotoreceptor retinoid-binding protein gene. *J Neurosci* **18**(12): 4511-4520.

Liu, L. and Gudas, L.J. 2005. Disruption of the lecithin:Retinol acyltransferase gene makes mice more susceptible to vitamin A deficiency. *J Biol Chem*.

Lorenz, B., Gyurus, P., Preising, M., Bremser, D., Gu, S., Andrassi, M., Gerth, C., and Gal, A. 2000. Early-onset severe rod-cone dystrophy in young children with RPE65 mutations. *Invest Ophthalmol Vis Sci* **41**(9): 2735-2742.

Lorenz, B., Wabbels, B., Wegscheider, E., Hamel, C.P., Drexler, W., and Preising, M.N. 2004. Lack of fundus autofluorescence to 488 nanometers from childhood on in patients with early-onset severe retinal dystrophy associated with mutations in RPE65. *Ophthalmology* **111**(8): 1585-1594.

Lyubarsky, A.L., Savchenko, A.B., Morocco, S.B., Daniele, L.L., Redmond, T.M., and Pugh, E.N., Jr. 2005. Mole quantity of RPE65 and its productivity in the generation of 11-cis-retinal from retinyl esters in the living mouse eye. *Biochemistry* **44**(29): 9880-9888.

Ma, J., Xu, L., Othersen, D.K., Redmond, T.M., and Crouch, R.K. 1998. Cloning and localization of RPE65 mRNA in salamander cone photoreceptor cells1. *Biochim Biophys Acta* **1443**(1-2): 255-261.

Machida, S., Kondo, M., Jamison, J.A., Khan, N.W., Kononen, L.T., Sugawara, T., Bush, R.A., and Sieving, P.A. 2000. P23H rhodopsin transgenic rat: correlation of retinal function with histopathology. *Invest Ophthalmol Vis Sci* **41**(10): 3200-3209.

Maeda, A., Maeda, T., Imanishi, Y., Kuksa, V., Alekseev, A., Bronson, J.D., Zhang, H., Zhu, L., Sun, W., Saperstein, D.A., Rieke, F., Baehr, W., and Palczewski, K. 2005. Role of photoreceptor-specific retinol dehydrogenase in the retinoid cycle in vivo. *J Biol Chem* **280**(19): 18822-18832.

Mata, N.L., Radu, R.A., Clemmons, R.C., and Travis, G.H. 2002. Isomerization and oxidation of vitamin a in cone-dominant retinas: a novel pathway for visual-pigment regeneration in daylight. *Neuron* **36**(1): 69-80.

Moiseyev, G., Chen, Y., Takahashi, Y., Wu, B.X., and Ma, J.X. 2005. RPE65 is the isomerohydrolase in the retinoid visual cycle. *Proc Natl Acad Sci U S A* **102**(35): 12413-12418.

Nicoletti, A., Wong, D.J., Kawase, K., Gibson, L.H., Yang-Feng, T.L., Richards, J.E., and Thompson, D.A. 1995. Molecular characterization of the human gene encoding an abundant 61 kDa protein specific to the retinal pigment epithelium. *Hum Mol Genet* **4**(4): 641-649.

Osterberg, G. 1935. Topography of the layer of rods and cones in the human retina. *Acta Ophthal(suppl)* **6**: 1-103.

Pang, J.J., Chang, B., Hawes, N.L., Hurd, R.E., Davisson, M.T., Li, J., Noorwez, S.M., Malhotra, R., McDowell, J.H., Kaushal, S., Hauswirth, W.W., Nusinowitz, S., Thompson, D.A., and Heckenlively, J.R. 2005. Retinal degeneration 12 (rd12): a new, spontaneously arising mouse model for human Leber congenital amaurosis (LCA). *Mol Vis* **11**: 152-162.

Paunescu, K., Wabbels, B., Preising, M.N., and Lorenz, B. 2005. Longitudinal and cross-sectional study of patients with early-onset severe retinal dystrophy associated with RPE65 mutations. *Graefes Arch Clin Exp Ophthalmol* **243**(5): 417-426.

Poliakov, E., Gentleman, S., Cunningham, F.X., Jr., Miller-Ihli, N.J., and Redmond, T.M. 2005. Key role of conserved histidines in recombinant mouse beta-carotene 15,15'-monooxygenase-1 activity. *J Biol Chem* **280**(32): 29217-29223.

Redmond, T.M. and Hamel, C.P. 2000. Genetic analysis of RPE65: from human disease to mouse model. *Methods Enzymol* **316**: 705-724.

Redmond, T.M., Poliakov, E., Yu, S., Tsai, J.Y., Lu, Z., and Gentleman, S. 2005. Mutation of key residues of RPE65 abolishes its enzymatic role as isomerohydrolase in the visual cycle. *Proc Natl Acad Sci U S A* **102**(38): 13658-13663.

Redmond, T.M., Yu, S., Lee, E., Bok, D., Hamasaki, D., Chen, N., Goletz, P., Ma, J.X., Crouch, R.K., and Pfeifer, K. 1998. Rpe65 is necessary for production of 11-cis-vitamin A in the retinal visual cycle. *Nat Genet* **20**(4): 344-351.

Reme, C.E., Wirz-Justice, A., and Terman, M. 1991. The visual input stage of the mammalian circadian pacemaking system: I. Is there a clock in the mammalian eye? *J Biol Rhythms* **6**(1): 5-29.

Rohrer, B., Lohr, H.R., Humphries, P., Redmond, T.M., Seeliger, M.W., and Crouch, R.K. 2005. Cone Opsin Mislocalization in Rpe65-/- Mice: A Defect That Can Be Corrected by 11-cis Retinal. *Invest Ophthalmol Vis Sci* **46**(10): 3876-3882.

Saari, J.C. 2000. Biochemistry of visual pigment regeneration: the Friedenwald lecture. *Invest Ophthalmol Vis Sci* **41**(2): 337-348.

Saari, J.C. and Bredberg, D.L. 1989. Lecithin:retinol acyltransferase in retinal pigment epithelial microsomes. *J Biol Chem* **264**(15): 8636-8640.

Saari, J.C., Bredberg, L., and Garwin, G.G. 1982. Identification of the endogenous retinoids associated with three cellular retinoid-binding proteins from bovine retina and retinal pigment epithelium. *J Biol Chem* **257**(22): 13329-13333.

Saari, J.C., Nawrot, M., Kennedy, B.N., Garwin, G.G., Hurley, J.B., Huang, J., Possin, D.E., and Crabb, J.W. 2001. Visual cycle impairment in cellular retinaldehyde binding protein (CRALBP) knockout mice results in delayed dark adaptation. *Neuron* **29**(3): 739-748.

Samardzija, M., Wenzel, A., Thiersch, M., Frigg, R., Reme, C., and Grimm, C. 2006. Caspase-1 Ablation Protects Photoreceptors in a Model of Autosomal Dominant Retinitis Pigmentosa. *Invest Ophthalmol Vis Sci* **47**(12): 5181-5190.

Scheel, J.R., Garrett, L.J., Allen, D.M., Carter, T.A., Randolph-Moore, L., Gambello, M.J., Gage, F.H., Wynshaw-Boris, A., and Barlow, C. 2003. An inbred 129SvEv GFPCre transgenic mouse that deletes loxP-flanked genes in all tissues. *Nucleic Acids Res* **31**(10): e57.

Schneeweis, D.M. and Schnapf, J.L. 1995. Photovoltage of rods and cones in the macaque retina. *Science* **268**(5213): 1053-1056.

Seeliger, M.W., Grimm, C., Stahlberg, F., Friedburg, C., Jaissle, G., Zrenner, E., Guo, H., Reme, C.E., Humphries, P., Hofmann, F., Biel, M., Fariss, R.N., Redmond, T.M., and Wenzel, A. 2001. New views on RPE65 deficiency: the rod system is the source of vision in a mouse model of Leber congenital amaurosis. *Nat Genet* **29**(1): 70-74.

Simon, A., Hellman, U., Wernstedt, C., and Eriksson, U. 1995. The retinal pigment epithelial-specific 11-cis retinol dehydrogenase belongs to the family of short chain alcohol dehydrogenases. *J Biol Chem* **270**(3): 1107-1112.

Sung, C.H., Davenport, C.M., Hennessey, J.C., Maumenee, I.H., Jacobson, S.G., Heckenlively, J.R., Nowakowski, R., Fishman, G., Gouras, P., and Nathans, J. 1991. Rhodopsin mutations in autosomal dominant retinitis pigmentosa. *Proc Natl Acad Sci U S A* **88**(15): 6481-6485.

Takahashi, Y., Chen, Y., Moiseyev, G., and Ma, J.X. 2006. Two point mutations of RPE65 from patients with retinal dystrophies decrease the stability of RPE65 protein and abolish its isomerohydrolase activity. *J Biol Chem* **281**(31): 21820-21826.

Takahashi, Y., Moiseyev, G., Chen, Y., and Ma, J.X. 2005. Identification of conserved histidines and glutamic acid as key residues for isomerohydrolase activity of RPE65, an enzyme of the visual cycle in the retinal pigment epithelium. *FEBS Lett* **579**(24): 5414-5418.

Thompson, D.A., Gyurus, P., Fleischer, L.L., Bingham, E.L., McHenry, C.L., Apfelstedt-Sylla, E., Zrenner, E., Lorenz, B., Richards, J.E., Jacobson, S.G., Sieving, P.A., and Gal, A. 2000. Genetics and phenotypes of RPE65 mutations in inherited retinal degeneration. *Invest Ophthalmol Vis Sci* **41**(13): 4293-4299.

Trehan, A., Canada, F.J., and Rando, R.R. 1990. Inhibitors of retinyl ester formation also prevent the biosynthesis of 11-cis-retinol. *Biochemistry* **29**(2): 309-312.

Van Hooser, J.P., Aleman, T.S., He, Y.G., Cideciyan, A.V., Kuksa, V., Pittler, S.J., Stone, E.M., Jacobson, S.G., and Palczewski, K. 2000. Rapid restoration of visual pigment

and function with oral retinoid in a mouse model of childhood blindness. *Proc Natl Acad Sci U S A* **97**(15): 8623-8628.

Van Hooser, J.P., Liang, Y., Maeda, T., Kuksa, V., Jang, G.F., He, Y.G., Rieke, F., Fong, H.K., Detwiler, P.B., and Palczewski, K. 2002. Recovery of visual functions in a mouse model of Leber congenital amaurosis. *J Biol Chem* **277**(21): 19173-19182.

Weng, J., Mata, N.L., Azarian, S.M., Tzekov, R.T., Birch, D.G., and Travis, G.H. 1999. Insights into the function of Rim protein in photoreceptors and etiology of Stargardt's disease from the phenotype in abcr knockout mice. *Cell* **98**(1): 13-23.

Wenzel, A., Grimm, C., Samardzija, M., and Reme, C.E. 2003. The genetic modifier Rpe65Leu(450): effect on light damage susceptibility in c-Fos-deficient mice. *Invest Ophthalmol Vis Sci* **44**(6): 2798-2802.

Wenzel, A., Oberhauser, V., Pugh, E.N., Jr., Lamb, T.D., Grimm, C., Samardzija, M., Fahl, E., Seeliger, M.W., Reme, C.E., and von Lintig, J. 2005. The retinal G protein-coupled receptor (RGR) enhances isomerohydrolase activity independent of light. *J Biol Chem* **280**(33): 29874-29884.

Wenzel, A., Reme, C.E., Williams, T.P., Hafezi, F., and Grimm, C. 2001. The Rpe65 Leu450Met variation increases retinal resistance against light-induced degeneration by slowing rhodopsin regeneration. *J Neurosci* **21**(1): 53-58.

Woodruff, M.L., Wang, Z., Chung, H.Y., Redmond, T.M., Fain, G.L., and Lem, J. 2003. Spontaneous activity of opsin apoprotein is a cause of Leber congenital amaurosis. *Nat Genet* **35**(2): 158-164.

Young, R.W. 1971. Shedding of discs from rod outer segments in the rhesus monkey. *J Ultrastruct Res* **34**(1): 190-203.

Zernant, J., Kulm, M., Dharmaraj, S., den Hollander, A.I., Perrault, I., Preising, M.N., Lorenz, B., Kaplan, J., Cremers, F.P., Maumenee, I., Koenekoop, R.K., and Allikmets, R. 2005. Genotyping microarray (disease chip) for leber congenital amaurosis: detection of modifier alleles. *Invest Ophthalmol Vis Sci* **46**(9): 3052-3059.

Znoiko, S.L., Crouch, R.K., Moiseyev, G., and Ma, J.X. 2002. Identification of the RPE65 protein in mammalian cone photoreceptors. *Invest Ophthalmol Vis Sci* **43**(5): 1604-1609.

Znoiko, S.L., Rohrer, B., Lu, K., Lohr, H.R., Crouch, R.K., and Ma, J.X. 2005. Downregulation of cone-specific gene expression and degeneration of cone photoreceptors in the Rpe65-/- mouse at early ages. *Invest Ophthalmol Vis Sci* **46**(4): 1473-1479.

ABBREVIATIONS

11cRDH	*11-cis retinol dehydrogenase*
A	*Absorbance*
ABCR	*ATP-binding cassette retina*
ACO	*Apocarotenoid-15,15-oxygenase*
ADRP	*Autosomal dominant RP*
AMD	*Age-related macular degeneration*
app.	*Approximately*
ARRP	*Autosomal recessive RP*
ATP	*Adenosine triphosphate*
atRDH	*All-trans retinol dehydrogenase*
BF	*Factor B*
bp	*Base pair(s)*
BSA	*Bovine serum albumin*
^{o}C	*Degree Celsius*
C2	*Complement component 2*
Ca^{2+}	*Calcium*
cAMP	*Cyclic adenosine monophosphate*
casp-1	*Caspase-1*
CD	*Cone dystrophy*
cd	*Candela*
cDNA	*Complementary deoxyribonucleic acid*
CFH	*Complement factor H*
cGMP	*Cyclic guanosine monophosphate*
CNG	*Cyclic-nucleotide-gated channels*
CRALBP	*Cellular retinaldehyde binding protein*
CRBP	*Cellular retinol binding protein*
CRD	*Cone-rod dystrophy*
CSNB	*Congenital stationary night blindness*
div.	*Division*
DNA	*Deoxynucleic acid*
dNTP	*Deoxynucleotide*
DT	*Diphtheria toxin*
dT	*Deoxytimidine*
EOSRD	*Early-onset severe retinal dystrophy*
ERG	*Electroretinogram*
ES	*Embryonic stem*
EtOH	*Ethanol*

FGF2	*Fibroblast growth factor 2*
FITC	*Fluorescein isothiocyanate*
GC	*Guanylate cyclase*
GCAP	*Guanylate-cyclase-activating protein*
GCL	*Ganglion cell layer*
GDP	*Guanosine diphosphate*
GFAP	*Glial fibrillary acidic protein*
GMP	*Guanosine monophosphate*
GNAT1	*Guanine nucleotide binding protein (G protein), alpha transducing activity polypeptide 1*
GNAT2	*Guanine nucleotide binding protein (G protein), alpha transducing activity polypeptide 2*
GTP	*Guanosine triphosphate*
h	*Hour*
HPLC	*High performance liquid chromatography*
HR	*Homologous recombination*
IMH	*Isomerohydrolase*
INL	*Inner nuclear layer*
IPL	*Inner plexiform layer*
IRBP	*Inter-photoreceptor retinol binding protein*
IS	*Inner segments*
ISI	*Inter-stimulus interval*
kb	*Kilo basepair(s)*
kDa	*Kilo Dalton*
KI	*Knock-in*
KO	*Knock-out*
LCA	*Leber congenital amaurosis*
loxP	*Locus of cross-over (x) in P1*
LRAT	*Lecithin retinol acyl transferase*
m	*Mili*
mcd*s/m^2	*Mili candela second per square meter*
MD	*Macular degeneration*
MerTK	*C-mer proto-oncogene tyrosine kinase*
min	*Minute(s)*
mRNA	*Messenger ribonucleic acid*
MWL	*Middle wavelength*
µF	*Micro faraday*
µV	*Micro volt*
µg	*Micrograms*
NADP	*Oxidized nicotinamide adenine dinucleotide phosphate*
NADPH	*Reduced nicotinamide adenine dinucleotide phosphate*

neo	*Neomycin*
NGS	*Normal goat serum*
NHS	*Normal horse serum*
nm	*Nanometer*
OCT	*Optical coherence tomography*
OLM	*Outer limiting membrane*
OMIM	*Online Mendelian inheritance in man*
ONL	*Outer nuclear layer*
OPL	*Outer plexiform layer*
OS	*Outer segments*
PBS	*Phosphate buffered saline*
PBST	*Phosphate buffered saline-triton*
PCR	*Polymerase chain reaction*
PDE	*Phosphodiesterase*
PFA	*Paraformaldehyde*
pmol	*Picomol*
rd12	*Retinal degeneration 12*
RFLP	*Restriction fragment length polymorphism*
RGR	*Retinal G-protein-coupled receptor*
Rho	*Rhodopsin*
RK	*Rhodopsin kinase*
RNA	*Ribonucleic acid*
RP	*Retinitis pigmentosa*
RPE	*Retinal pigment epithelium*
RPE65	*Retinal pigment epithelium-specific protein 65kDa*
RT	*Room temperature*
S.D.	*Standard deviation*
SDS	*Sodium dodecyl sulfate*
sec	*Second*
Stgdt	*Stargardt*
SWL	*Short wavelength*
UV	*Ultraviolet*
V	*Volt*
wks	*Weeks*
wt	*Wild-type*
XLRS	*X-linked retinoschisis*

ACKNOWLEDGMENTS

I would like to thank Prof. Dr. Charlotte Remé for her support and encouragement, and for offering me the opportunity to conduct research work towards my doctoral thesis in her group. Prof. Dr. Peter Sonderegger and Prof. Dr. Jean-Marc Fritschy are kindly acknowledged for accepting to referee this thesis.

I am particularly grateful to PD Dr. Christian Grimm and PD Dr. Andreas Wenzel. Each with his own expertise, Christian and Andreas gave me the freedom to explore on my own, yet always being available to assist me at all stages of my work. Only a few PhD students are lucky to experience such support.

Furthermore, my gratitude goes to:

PD Dr. Johannes von Lintig and Dr. Vitus Oberhouser for their generous help with HPLC analyses and Johannes's critical reading of the discussion.

PD Dr. M. Seeliger and Dr. Naoyuki Tanimoto for their expertise in the mysterious ways of ERG.

Dr. Corinne Kostic for her help with immunohistochemistry.

Sarah Habegger, Karsten Stauffer and BZL affiliates who provided excellent service with animal husbandry and embryo transfer.

All the current and former members of our laboratory for their practical and personal support.

Mario, who has supported me throughout this period, for understanding my physical, and often, mental absence.

CURRICULUM VITAE

Family Name	Samardzija
First name	Marijana
Date of birth:	November 5, 1971
Nationality:	Croatian
Address:	Wilstrasse 15, 8610 Uster, Switzerland
e-mail:	marijana.samardzija@opht.unizh.ch

EDUCATION AND EXPERIENCE:

December 2001- present PhD student in the Laboratory for Retinal Cell Biology, Ophthalmology, University Hospital Zurich

November 1999 – June 2001 Research assistant at Institute of Medical Biochemistry, Karl-Franzens University Graz, Austria

May 1997 - November 1999 Research assistant at Department of Molecular Biology, Faculty of Natural Science University of Zagreb

1997 Graduated Molecular Biology at Faculty of Natural Sciences, University of Zagreb:

RELEVANT COURSES:

Biotechnology Workshop: New Gene Discovery presented by Exon-Intron at Penn State University; September 18-22, 2000, Graz, Austria

LTK Module 9: Targeted mutagenesis in mouse; January 16-18, 2002, Zurich, Switzerland

LTK Module 1: Introductory course in laboratory animal science; March 18-22, 2002, Zurich, Switzerland

EMBnet Course: Introduction to Bioinformatics; October 11-15, 2004, Zurich, Switzerland

UNI ETH Sprachzentrum: Writing English for Science; Nov-Dec, 2004, Zurich Switzerland

Participated in the ZNZ Ph.D. program (Neuroscience Centre Zurich)

CONGRESSES AND SYMPOSIA:

The Sixth Congress of Croatian Biologists, Opatija, Croatia; 1997

First Congress of Croatian Geneticist, June 1-4, Hvar, Croatia; 1998

FASEB Summer Research Conferences: Calcium and Cell Function, July 9-14, Copper Mountain, Colorado, USA; 2000

ARVO Annual Meeting, May 5-10, Fort Lauderdale, Florida, USA; 2002

Xth International Symposium on Retinal Degeneration September 30-October 5, Bürgenstock, Switzerland; 2002

ARVO Annual Meeting, May, Fort Lauderdale, Florida, USA; 2003

3rd Day of Clinical Research, USZ, Zürich; 2004

ARVO Annual Meeting, May, Fort Lauderdale, Florida, USA; 2004

ZNZ Symposium 2004, Neuroscience Center Zurich.

ARVO Annual Meeting, May, Fort Lauderdale, Florida, USA; 2005

4th Day of Clinical Research, USZ, Zürich; 2005

ZNZ Symposium 2005, Neuroscience Center Zurich.

The Swiss Retina Meeting, Brunnen; 2005

5th Day of Clinical Research, USZ, Zürich; 2005

ZIHP Symposium 2006, Zürich

ZNZ Symposium 2006, Neuroscience Center Zurich.

PUBLICATIONS

1. Besendorfer, V., Samardzija, M., Busic, M., Solic, M. E., and Papes, D. (1997) Periodicum Biologorum 99, 415-421
2. Besendorfer, V., Samardzija, M., Zoldos, V., Solic, M. E., and Papes, D. (2002) Botanical Journal of the Linnean Society 139(1), 99-108
3. Frieden, M., Malli, R., Samardzija, M., Demaurex, N., and Graier, W. F. (2002) J Physiol 540(Pt 1), 73-84
4. Grimm, C., Wenzel, A., Groszer, M., Mayser, H., Seeliger, M., Samardzija, M., Bauer, C., Gassmann, M., and Reme, C. E. (2002) Nat Med 8(7), 718-724
5. Wenzel, A., Grimm, C., Samardzija, M., and Reme, C. E. (2003) Invest Ophthalmol Vis Sci 44(6), 2798-2802
6. Grimm, C., Wenzel, A., Stanescu, D., Samardzija, M., Hotop, S., Groszer, M., Naash, M., Gassmann, M., and Reme, C. (2004) J Neurosci 24(25), 5651-5658
7. Seeliger, M. W., Beck, S. C., Pereyra-Munoz, N., Dangel, S., Tsai, J. Y., Luhmann, U. F., van de Pavert, S. A., Wijnholds, J., Samardzija, M., Wenzel, A., Zrenner, E., Narfstrom, K., Fahl, E., Tanimoto, N., Acar, N., and Tonagel, F. (2005) Vision Res 45(28), 3512-3519
8. Wenzel, A., Grimm, C., Samardzija, M., and Reme, C. E. (2005) Prog Retin Eye Res 24(2), 275-306
9. Wenzel, A., Oberhauser, V., Pugh, E. N., Jr., Lamb, T. D., Grimm, C., Samardzija, M., Fahl, E., Seeliger, M. W., Reme, C. E., and von Lintig, J. (2005) J Biol Chem 280(33), 29874-29884
10. Frigg, R., Wenzel, A., Samardzija, M., Oesch, B., Wariwoda, H., Navarini, A. A., Seeliger, M. W., Tanimoto, N., Reme, C., and Grimm, C. (2006) Exp Eye Res 83(6), 1350-1358
11. Samardzija, M., Wenzel, A., Aufenberg, S., Thiersch, M., Reme, C., and Grimm, C. (2006) Faseb J 20(13), 2411-2413
12. Samardzija, M., Wenzel, A., Naash, M., Reme, C. E., and Grimm, C. (2006) Eur J Neurosci 23(4), 1028-1034
13. Samardzija, M., Wenzel, A., Thiersch, M., Frigg, R., Reme, C., and Grimm, C. 2006. Invest Ophthalmol Vis Sci 47(12): 5181-5190.